Available online at www.sciencedirect.com
ScienceDirect
Journal of the Mechanics and Physics of Solids 56 (2008) 1484–1510
JOURNAL OF THE MECHANICS AND PHYSICS OF SOLIDS
www.elsevier.com/locate/jmps

A bio-mechanical model for coupling cell contractility with focal adhesion formation

Vikram S. Deshpande[a,c,*], Milan Mrksich[b], Robert M. McMeeking[c], Anthony G. Evans[c]

[a]*Department of Engineering, University of Cambridge, Trumpington Street, Cambridge CB2 1PZ, UK*
[b]*Howard Hughes Medical Institute/Department of Chemistry, University of Chicago, Chicago, IL 60637, USA*
[c]*Mechanical Engineering Department and Materials Department, University of California, Santa Barbara, CA 93106, USA*

Received 15 April 2007; received in revised form 9 August 2007; accepted 15 August 2007

Abstract

Focal adhesions (FAs) are large, multi-protein complexes that provide a mechanical link between the cytoskeletal contractile machinery and the extracellular matrix. They exhibit mechanosensitive properties; they self-assemble upon application of pulling forces and dissociate when these forces are decreased. We rationalize this mechano-sensitivity from thermodynamic considerations and develop a continuum framework in which the cytoskeletal contractile forces generated by stress fibers drive the assembly of the FA multi-protein complexes. The FA model has three essential features: (i) the low and high affinity integrins co-exist in thermodynamic equilibrium, (ii) the low affinity integrins within the plasma membrane are mobile, and (iii) the contractile forces generated by the stress fibers are in mechanical equilibrium and change the free energies of the integrins. A general two-dimensional framework is presented and the essential features of the model illustrated using one-dimensional examples. Consistent with observations, the coupled stress fiber and FA model predict that (a) the FAs concentrate around the periphery of the cell; (b) the fraction of the cell covered by FAs increases with decreasing cell size while the total FA intensity increases with increasing cell size; and (c) the FA intensity decreases substantially when cell contractility is curtailed.

Keywords: Mechano-sensitivity; Self-assembly; Focal adhesions; Stress fibers; Myosin.

1. Introduction

Cells interact with substrates coated with extracellular matrix proteins (ECM) through the formation of multi-molecular complexes referred to as focal adhesions (FAs). The FAs form the mechanical link between the cytoskeleton within the cell and the ECM. They are typically 1–3 μm in extent. The FA comprises a layer of trans-membrane integrin molecules and a multi-protein sub-membrane plaque. The integrins are integral membrane hetero-dimeric proteins with extracellular domains that bind to ligands attached to the substrate, as

*Corresponding author.
E-mail address: vsd@eng.cam.ac.uk (V.S. Deshpande).

0022-5096/$ - see front matter © 2007 Elsevier Ltd. All rights reserved.
doi:10.1016/j.jmps.2007.08.006

well as intracellular domains that provide docking sites for the assembly of the plaque. In turn, the plaque consists of many different proteins including talin, α-actinin, filamin, FA kinase, vinculin, paxillin, and tensin. Some of these proteins form the structural scaffold of the adhesion site, while others mediate signaling processes. This FA plaque also serves as a platform for nucleation and development of stress fibers within the cell (bundles of actin filaments containing myosin and various actin-binding proteins). The stress fibers are major generators of intracellular contractile forces, transmitted through the FA plaque and the integrins to the substrate. Namely, there is an intimate linkage between the formation of the FAs around the cell periphery and the development of stress fibers within the cell. To characterize and predict the bio-chemo-mechanical interactions between a cell and the ECM, a model must be devised that incorporates the influence of the forces exerted by the stress fibers on the formation of FA. Developing such a model is the primary intent of this article. The FA component of the model will be intimately linked with a cell contractility scheme developed by Deshpande et al. (2006, 2007) that characterizes the organization of the stress fibers and the tractions they exert on the substrate.

A growing body of experimental evidence suggests that FA formation is itself controlled mechanically, with the tractions generated at the contact sites increasing the rate of assembly of the FAs (Balaban et al., 2001; Tan et al., 2003; Petroll et al., 2003). Recent results (Parker et al., 2002; Brock et al., 2003; Chen et al., 2003) also demonstrate that the global shape of cells and their internal cytoskeletal structure play an important role in constraining the magnitude, distribution, and direction of such tractions across the cell surface, and thereby control local FA assembly and organization. In particular, stationary cells tend to organize long stress fibers, with large FAs concentrating at the cell periphery (Fig. 1a) and in high curvature regions. Moreover, FA formation also can be increased or decreased by, respectively, raising or lowering the cytoskeletal tension, using pharmacological agents that curtail acto-myosin activity (Fig. 1b). A number of important questions arise from these observations. Does an adhesion/stress fiber interaction leads to this self-organizing behavior, with the FAs concentrating at the cell periphery? What determines the time-scale of FA redistribution? Following the pioneering studies of Bell (1978) and Bell et al. (1984), Dembo et al. (1988) described adhesion

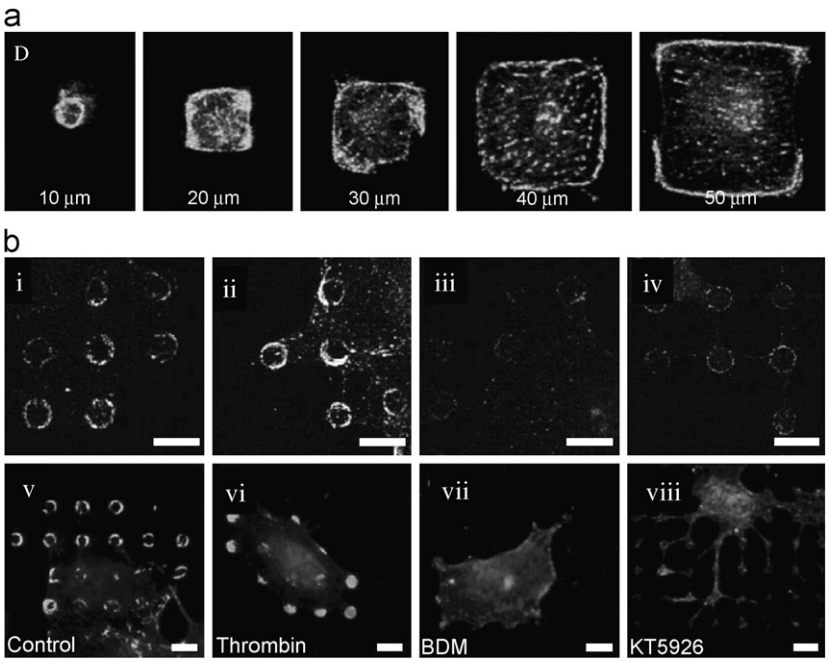

Fig. 1. (a) Fluorescent confocal micrographs of individual, vinculin-labeled Bovine capillary endothelial cells cultured on square islands of different sizes (lengths of sides are indicated). (b) Immunofluorescence images of vinculin in Bovine capillary endothelial cell (i–iv) and Human vascular endothelial cells (v–viii) cells on 5 μm islands that were untreated (i, v) or exposed to thrombin (ii, vi), BDM (iii, vii), or KT5926 (iv, viii). Scale bars indicate a 10 μm length. Reproduced from Chen et al. (2003).

by a chemical rate reaction theory, whereas Evans (1985) employed a traditional cohesive zone approach. Freund and Lin (2004) investigated the role of binder mobility in the development of adhesive contacts.

Because FAs contain components that interact with a large number of signaling cascades (Burridge and Chrzanowska-Wodnicka, 1996), shape-regulated FA formation could provide a molecular mechanism for how cell structure and physical distortion of cell shape can be transduced into biochemical signals inside the cell. Thus, this inside—out regulation of FA assembly may be critical in integrating many physical cues—cell shape, ECM compliance, intracellular tension, and cytoskeletal architecture—into signals that partially determine cell function. The fact that many proteins perform both structural and signaling functions hinders the ability of traditional genetic approaches to parse the mechanisms that regulate FA dynamics, since knocking out a protein by genetic manipulation may also eliminate an essential structural component. Consequently, to understand how specific molecular features give rise to the observed behavior it is essential to combine experimental studies of adherent cells—including the use of microscopy to observe the structure and dynamics of the cytokskeleton and FAs—with computational models that include the salient mechanics.

A generalized model must be capable of characterizing the assembly of the FAs in terms of the basic interactions between the forces, the assembly and dissolution of stress fibers and the compliance of the substrate. Moreover, once calibrated, it must explain such effects as the preference for FA formation at the cell periphery, the strong influence of substrate compliance on the forces exerted on the substrate, the influence of cell size on FA formation and on the magnitude of the forces, as well the influence of cell shape and boundary conditions on the orientations of the fibers. Although the nature of mechanical sensing by FA is not fully understood, several possible mechanisms have been proposed (Bershadsky et al., 2003; Zhu et al., 2000) and a number of phenomenological models have been developed that account for the growth of FAs with increasing traction forces at the adhesion sites (Novak et al., 2004, Nicolas et al., 2004; Nicolas and Safran, 2006). All of these models assume a-priori that traction forces developed at the contact sites increase the rate of assembly of focal adhesions and have the limitation that they do not present a consistent thermodynamic framework. Furthermore, these models either just take into account elastic stresses developed in the cell (Nicolas et al., 2004; Nicolas and Safran 2006) or assume an ad hoc relation for the forces generated by acto/myosin stress fibers (Novak et al., 2004; Shemesh et al., 2005). Here we pursue a mechano-sensitive model of the processes that form FAs. The model incorporates contributions to the free energies of the integrins from the stored energy caused by stretching of the integrin–ligand complexes and the potential energy due to the mechanical work done by the cytoskeleton—it is the combination of these two contributions that governs the stability of the receptor–ligand complex. This model is then coupled with a biochemically motivated stress fiber model (Deshpande et al., 2006, 2007) that accurately predicts a large number of observations including: (i) the scaling of forces generated by cells on a bed of microneedles (Deshpande et al., 2007); (ii) the sensitivity of the contractile response to the stiffness of the substrate (Deshpande et al., 2006), and (iii) the evolution of stress fiber orientations in cells subjected to cyclic stretch (Wei et al., 2007). It will be shown that the new, integrated model is capable of rationalizing many experimental observations of FA formation.

The article is organized in the following manner. First, the basic observations of FA formation are summarized as a motivation for the modeling approach. This is followed by a description of the model in terms of the chemical potentials and the fluxes. Thereafter, the application of the model in one dimension is presented in three parts. In the first, the parameters to be used in the model are summarized. Then two single cell phenomena are analyzed. One examines a cell on an ''infinite'' substrate. The other addresses a cell on a patterned substrate. In both cases, the predictions of FA formation are compared with experimental observations. Finally, an example of the implementation of the model in two dimensions is presented for a cell on a stiff substrate with a V-shaped micro-patterned ligand patch. Additional two-dimensional examples are presented in a companion article (Pathak et al., 2007).

2. Brief review of the biochemistry of the binding proteins (integrins)

Integrin proteins enable a bidirectional control of cell adhesion, by dynamically coupling the immobilized matrix and its associated ligands outside the cell with its internal ''skeleton''. Recent studies (Xiao et al., 2004) have elucidated that integrins exist in two conformational states: (i) a low affinity (or bent) state and (ii) an active or ''straight'' state with a high affinity to the appropriate ligand (see Fig. 2); see Carman and Springer

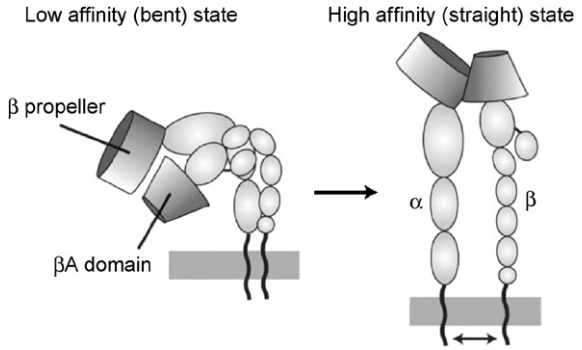

Fig. 2. The two conformational states of integrins. (a) The low affinity (inactive or bent) conformation and (b) the high affinity (active or straight conformation). Reproduced from Lodish et al. (2004).

(2003) for a detailed review. The high affinity integrins interact with the ligand molecules on the ECM and form complexes or bonds. The complexes have equilibrium dissociation constants in the low to high micromolar range and thus are weak compared to metallic or covalent bonds (Hynes, 1992). In conjunction with the time dependence of the bonding process, this magnitude of interaction is important in achieving the reversibility that is essential for sustaining the life of an organism. It must be possible to make or break chemical bonds by means of catalytic agents, small temperature changes and small mechanical forces. The "bent" geometry of the low affinity integrins implies that they do not interact with ligand molecules on the ECM.

Three sets of observations imply that the clustering of the integrins is driven by the contractile apparatus *within the cell* (Burridge and Chrzanowska-Wodnicka, 1996), and *not from interactions with the ECM on the outside*. The clustering is weak or non-existent if (i) the protein that signals the formation of the contractile stress fibers (Rho) is inactive (Hotchin and Hall, 1995), (ii) 2,3-butanedione monoxime (BDM) is added to the cell to restrict the actin–myosin activity (Chen et al., 2003) (Fig. 1b), and (iii) the concentration of FA proteins (such as vinculin) is maximum around the periphery of stationary cells (Fig. 1a) where the tractions exerted by the stress fibers on the ECM are at their maximum (Parker et al., 2002; Brock et al., 2003; Chen et al., 2003). The implication is that the binders migrate toward the regions of high traction by a diffusive process. However, no biochemical–mechanical basis for the mechano-sensitivity of the binders has been proposed. The ensuing article presents such a basis and derives a model capable of reproducing the foregoing observations as well as others in the literature.

3. A new biochemo-mechanical model for FA formation and growth

The ensuing model will characterize adhesion of a cell membrane containing binders or receptors (e.g. integrins) to a substrate with compatible ligands (e.g. the Arg–Gly–Asp ligand found in fibronectin). The substrate may be rigid or flexible and thus may be regarded either as a tissue or artificial substrate. The low affinity integrins are mobile within the plasma membrane. The high affinity integrins are connected to intracellular FA proteins (such as talin and vinculin) that link it to the cytoskeletal fibers. They are relatively stationary within the cell wall and modeled as immobile (it will be seen subsequently that the concentrations of the unbound high affinity integrins are sufficiently low that it is reasonable to neglect the diffusion of these types of binders).

Chemical Potentials. When in local equilibrium at a dilute concentration ξ_L,[1] the low affinity integrins have chemical potential:

$$\chi_L = \mu_L + kT \ln(\xi_L/\xi_R), \tag{1}$$

[1]In certain situations, such as in the presence of nano-scale clustered adhesion ligands, there may be an increase in the effective receptor–ligand affinity upon clustering. (Irvine et al., 2002). The dilute concentration assumptions implicit in Eqs. (1) and (2) are no longer valid in such situations and thus outside the scope of the present framework.

where μ_L is their reference chemical potential at the reference binder concentration ξ_R, k is the Boltzmann constant, and T the absolute temperature. The first term in Eq. (1) represents the contribution from the internal energy (enthalpy) and the second is the entropy of mixing (Gaskell, 1973). The "straight" configuration of high affinity integrins causes them to be less stable than the "bent" or low affinity state (Cluzel et al., 2005), implying that they have a higher reference potential $\mu_H > \mu_L$. Moreover, for geometrical reasons, only this straight form interacts with the ligand molecules on the ECM. Consequently, the chemical potential χ_H includes additional contributions from the stretching of the bonds:

$$\chi_H = \mu_H + kT \ln(\xi_H/\xi_R) + \Phi(\Delta_i) - F_i\Delta_i. \tag{2}$$

Here $\Phi(\Delta_i)$ is the stretch energy stored in the integrin-ligand complex, while the work-conjugate force, F_i, is related to the stretch Δ_i by

$$F_i = \frac{\partial \Phi}{\partial \Delta_i}. \tag{3}$$

The $-F_i\Delta_i$ term in Eq. (2) is the mechanical work term that represents the loss in free energy due to the stretch Δ_i of the integrin–ligand by the force F_i. (It is analogous to the pressure–volume term in the thermodynamics of gases.) In molecular terms, the stretch of the ligand–integrin bond stabilizes the adhesion complex by lowering the free energy χ_H. The formulae (1) through (3) are used widely to characterize the thermodynamic states of solids (Gaskell, 1973). The work term in Eq. (3) had been identified previously (Shemesh et al., 2005) as an important constituent of the thermodynamic state of the FAs. However, the terms due to the stored energy and the configurational entropy have been neglected in these prior assessments. Yet, they are critical constituents of a general thermodynamic framework that explicitly accounts for the cytoskeletal response, including remodeling as a result of contractility, spreading etc.

The kinetics governing the rate of conversion of the low affinity integrins to their high affinity state (and vice versa) are fast compared to all other time-scales involved, implying that the concentrations of the two forms of the integrins are governed by thermodynamic equilibrium. Namely, at each location x_i on the plasma membrane:

$$\chi_H = \chi_L. \tag{4}$$

Thus, in the absence of any interactions between the integrins and the ligand (an isolated cell with $F_i = 0$, $\Delta_i \to \infty$), the ratio of the steady-state concentrations of the low and high affinity integrins on the plasma membrane is

$$\frac{\xi_L}{\xi_H} = \exp\left[\frac{\mu_H - \mu_L}{kT} + \frac{\gamma}{kT}\right]. \tag{5}$$

Here $\gamma \equiv \Phi(\Delta_i \to \infty)$ is the surface energy of the high affinity integrins when sufficiently separated from the ligand that the interaction force is negligible. Ions (such as Mn^{2+}) reduce the surface energy γ and/or the difference in the reference chemical potential $\mu_H - \mu_L$ between the two integrin states causing the fraction present in the high affinity form to increase (Cluzel et al., 2005).

Most previous assessments (Bell, 1978; Bell et al., 1984; Dembo et al., 1988) considered only two states of the integrin molecules: bound or unbound. The chemical potentials described above clarify that, while the low affinity state is always unbound, with χ_L dependent only on the concentration, the state of the high affinity integrins depends upon the stretch of the integrin-ligand complex. This is illustrated in Fig. 3 where the chemical potentialχ_H is plotted as a function of the magnitude of the stretch $\Delta \equiv |\Delta_i|$ of the integrin–ligand complex. Consider the variation of χ_H with Δ for a given ξ_H. At $\Delta = 0$, the integrin is bound to the ligand but the complex is unstretched and thus has a chemical potential $\chi_H^B = \mu_H + kT \ln(\xi_H/\xi_R)$. With increasing stretch Δ, the force in the complex increases, thereby decreasing χ_H and stabilizing the complex. This continues until the force in the complex reaches a maximum value F_{max} at the stretch $\Delta = \Delta_{peak}$. With continued stretching, the force decreases and χ_H begins to rise: χ_H asymptotes to the value $\chi_H^U = \chi_H^B + \gamma$ when the force in the complex is zero and the integrin and ligand are widely separated. This corresponds to the unbound state of the high affinity integrin. As illustrated in Fig. 3 the chemical potential of the high

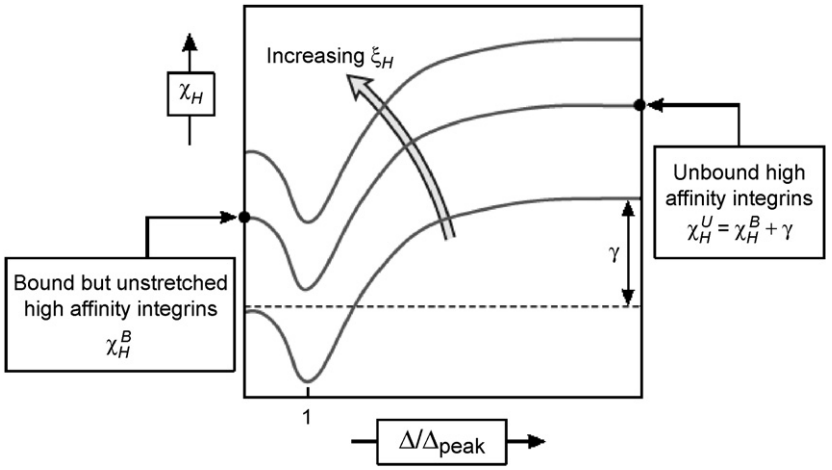

Fig. 3. An illustration of the effect of the stretch magnitude $\Delta \equiv |\Delta_i|$ on the chemical potential χ_H of the high affinity integrins. Curves are shown for three increasing values of the integrin concentration ξ_H and show that χ_H is a minimum when the interaction force between the integrin and the ligand is a maximum at a stretch $\Delta = \Delta_{peak}$.

affinity integrins also increases with increasing ξ_H due to the rise in the configurational entropy of the integrins.

Integrin Fluxes. The kinetics governing the rate of conversion of the low affinity integrins to their high affinity state (and vice versa) are assumed fast compared to all other time-scales involved (namely relative to the formation and dissociation of the stress fibers and the diffusion of the integrins along the cell wall). Thus the ratio of the low to high affinity integrin concentrations at any point on the plasma membrane is determined by Eq. (4) while the low affinity integrin fluxes along the plasma membrane are governed by a diffusive process. The spatial gradient in the chemical potential of the low affinity integrins imposes a driving force that biases their diffusional drift. In particular, the mean binder speed v_α along the cell membrane is proportional to the negative gradient in the chemical potential according to (Mullins, 1957)

$$v_\alpha = -m\frac{\partial \chi_L}{\partial x_\alpha}, \tag{6}$$

where m is a mobility parameter and the Greek subscripts (having the range 1,2) refer to a local set of Cartesian co-ordinates in the deformed cell membrane. The net flux j_α of these integrins across a section of the cell wall (positive in the direction of increasing x_α) is then

$$j_\alpha = \xi_L v_\alpha = -m\xi_L \frac{\partial \chi_L}{\partial x_\alpha}. \tag{7}$$

It remains to specify a conservation law relating the flux j_α to the local integrin concentration. Consider an elemental area of the cell wall, $dA = dx_1 dx_2$, with a density of integrins per unit area, $\xi = \xi_L + \xi_H$ (Fig. 4). The fluxes in and out of the area are shown in Fig. 4. Conservation of the number of binders dictates that

$$\begin{aligned}\frac{\partial}{\partial t}(\xi\, dx_1\, dx_2) = &\left[j_1(-dx_1/2, 0) - j_1(dx_1/2, 0)\right] dx_2 \\ &+ \left[j_2(0, -dx_2/2) - j_2(0, dx_2/2)\right] dx_1,\end{aligned} \tag{8}$$

which simplifies in the infinitesimal limit to

$$\frac{\partial \xi}{\partial t} = -\frac{\partial j_\alpha}{\partial x_\alpha} - \xi\frac{d\dot{A}}{dA}, \tag{9}$$

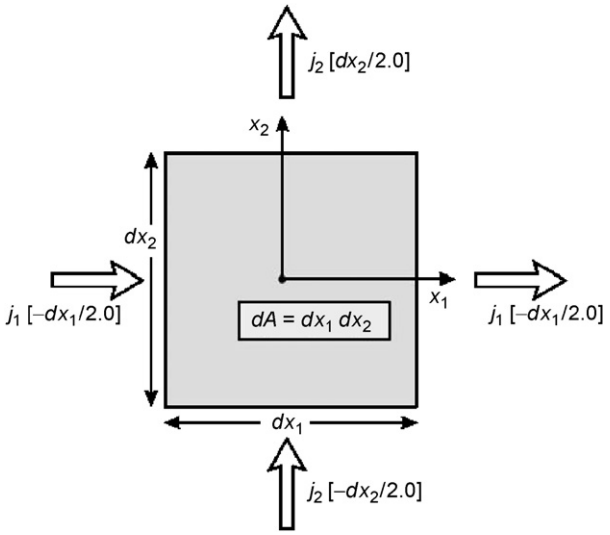

Fig. 4. The fluxes of integrins across an elemental area dA on the cell surface.

where the superposed dot indicates material differentiation with respect to time. The current area dA (with outward normal n_i) can be related to the corresponding un-deformed area dA_0 (with outward normal N_i) through the deformation gradient, $F_{ij} = \delta_{ij} + \partial u_i/\partial X_j$, where δ_{ij} is the Kronecker delta and $\partial u_i/\partial X_j$ are the spatial gradients of the cell displacements u_i with respect to the undeformed configuration. Here Non-Greek subscripts are employed to emphasize that the spatial gradients are defined with respect to a fixed three-dimensional Cartesian co-ordinate system. Nanson's formula states that (Malvern, 1969)

$$n_i\,\mathrm{d}A = JN_jF_{ji}^{-1}\,\mathrm{d}A_0, \tag{10}$$

where $J = \det(F_{ij})$. Differentiating (10) with respect to time gives

$$\frac{\mathrm{d}\dot{A}}{\mathrm{d}A} = \left(\frac{\partial \dot{u}_i}{\partial x_i}n_k - \frac{\partial \dot{u}_l}{\partial x_k}n_l - \dot{n}_k\right)n_k, \tag{11}$$

and thus the conservation law (9) reduces to

$$\frac{\partial \xi}{\partial t} = -\frac{\partial j_\alpha}{\partial x_\alpha} - \xi n_k\left(\frac{\partial \dot{u}_i}{\partial x_i}n_k - \frac{\partial \dot{u}_l}{\partial x_k}n_l - \dot{n}_k\right). \tag{12}$$

Eqs. (7) and (12) are the governing equations for the trafficking of the integrins along the cell wall, with the ratio ξ_L/ξ_H specified by Eq. (4).

Coupling with cytoskeletal response. The tractions T_i on the cell membrane (defined as the force per unit area on the cell surface) are dictated by the forces F_i on the integrin–ligand complexes, in combination with the concentrations of the high affinity integrins, in accordance with

$$T_i = -\xi_H F_i, \tag{13a}$$

where the minus sign arises because F_i are the forces that *the cell* exerts on the integrin–ligand complex. Since these tractions are balanced by the stresses within the cell, the coupling of cell contractility with adhesion involves the mechanical equilibrium equation

$$\Sigma_{ij,j} = 0, \tag{13b}$$

with traction boundary conditions $T_i = \Sigma_{ij}n_j = -\xi_H F_i$ over the cell membrane. Here Σ_{ij} are the Cauchy stresses within the cell specified by a model for the cell that accounts for cytoskeletal contractility (Deshpande

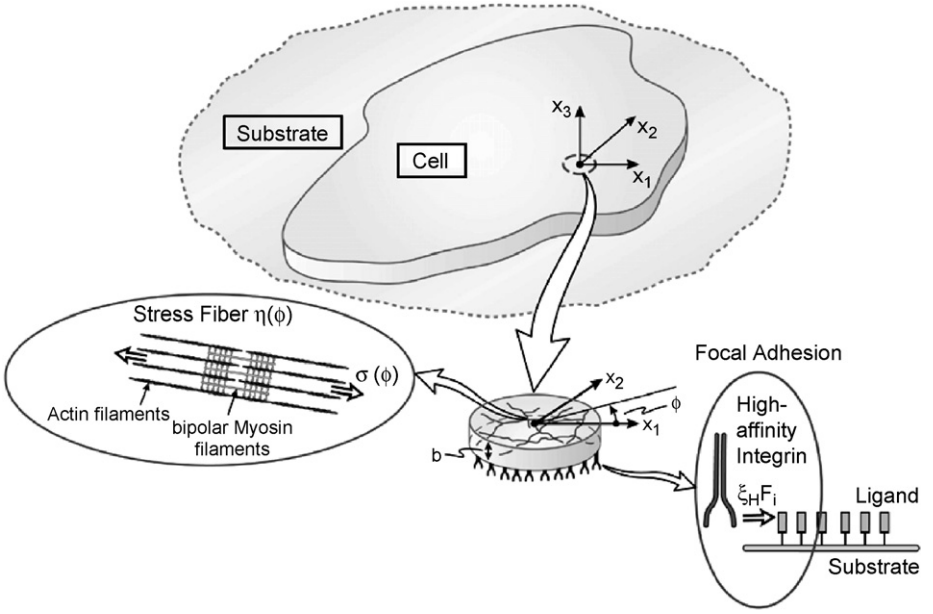

Fig. 5. Schematic representation of cell on a ligand coated substrate. The network of stress fibers and the integrin–ligand complex part of the focal adhesion are shown as insets.

et al., 2006, 2007). An example of this coupling is illustrated in Fig. 5 for a "two-dimensional" cell, thickness b in the x_1-x_2 plane, lying on a flat substrate having normal in the x_3-direction. One-dimensional solutions to such problems are detailed in Section 5.

The bond energies and interaction forces. We restrict attention to "sliding" interactions between a *flat* substrate (in the x_1-x_2 plane) and the cell and consider a simplified model for the interactions of the high affinity integrins with the ligand molecules.[2] The main restriction in choosing the functional $\Phi(\Delta_i)$ is that the integrin-ligand complexes have a finite rupture energy, such that

$$\gamma \equiv \Phi(\Delta_i \to \infty). \tag{14}$$

Henceforth the subscript i on the bond stretch components Δ_i takes only the values 1 and 2 as the bond stretches are defined in the plane of the flat substrate. Rather than employing a complex interaction (such as the Lennard-Jones (1931) potential), we utilize the simplest functional form for $\Phi(\Delta_i)$ that satisfies Eq. (14). We recognize that this simple form does not capture many of the details that accompany the energy landscape for dissociation, but does, as shown below, capture the essential physics of FA formation. Hence a simple piecewise quadratic potential is chosen (Fig. 6a):

$$\Phi = \begin{cases} (\frac{1}{2})\lambda_s\Delta_e^2, & \Delta_e \leqslant \Delta_n, \\ -\lambda_s\Delta_n^2 + 2\lambda_s\Delta_n\Delta_e - (\frac{1}{2})\lambda_s\Delta_e^2, & \Delta_n < \Delta_e \leqslant 2\Delta_n, \\ \lambda_s\Delta_n^2, & \Delta_e > 2\Delta_n, \end{cases} \tag{15a}$$

so that the surface energy, $\gamma \equiv \lambda_s\Delta_n^2$, with the effective stretch $\Delta_e \equiv \sqrt{\Delta_1^2 + \Delta_2^2}$ and λ_s is the stiffness of the bond. The maximum force, $\lambda_s\Delta_n$, occurs at a stretch $\Delta_e = \Delta_n$.

[2]The treatment presented here can be readily extended to more general interactions between the cell and an arbitrary-shaped substrate/ECM by choosing an appropriate bond energy functional Φ.

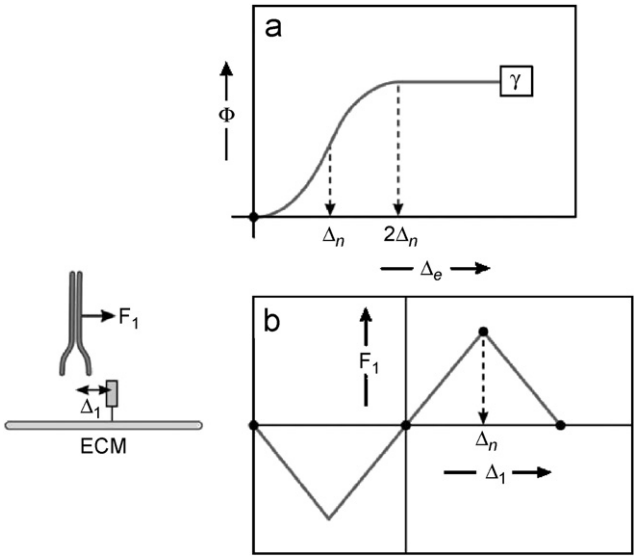

Fig. 6. Sketches of the (a) bond energy Φ as a function of the effective bond stretch Δ_e and (b) the corresponding bond force versus displacement relation with $\Delta_2 = 0$.

The corresponding forces for interactions between a *single isolated binder (integrin) and ligand molecule pair* are piecewise linear functions of Δ_i (Fig. 6b) and follow from Eq. (3) as

$$F_i = \begin{cases} \lambda_s \Delta_e \dfrac{\Delta_i}{\Delta_e}, & \Delta_e \leqslant \Delta_n \\ 2\lambda_s \Delta_n \dfrac{\Delta_i}{\Delta_e} - \lambda_s \Delta_e \dfrac{\Delta_i}{\Delta_e}, & \Delta_n < \Delta_e \leqslant 2\Delta_n, \\ 0, & \Delta_e > 2\Delta_n. \end{cases} \tag{15b}$$

In contrast, an integrin sliding over an ECM *with a high density of ligand molecules* (i.e. the spacing between the ligand molecules is much less than Δ_n) has a different force/displacement relation (Fig. 7a). The applied force thus starts at zero and increases with increasing displacement of the integrin to the right due to the interaction of the integrin with the first ligand molecule. The force reaches a peak at $\lambda_s \Delta_n$ and subsequently sliding of the cell membrane with respect to the substrate occurs at almost constant force. The physics of the integrin interactions with the ligand molecules leading to this response are discussed in Appendix A.

Since the high affinity integrins are fixed with respect to the cell membrane and the ligands are fixed to the ECM, we propose that, for integrins in contact with the ECM and located at x_i, the rate of evolution of the stretch of the integrin–ligand complex is related to the displacements of the cell by

$$\dot{\Delta}_i = \begin{cases} \dot{u}_i - \dot{u}_i^S, & \Delta_e \leqslant \Delta_n \ \text{ or } \ \left[\dfrac{\partial \Phi}{\partial \Delta_e}\dot{\Delta}_e < 0\right], \\ 0, & \text{otherwise}, \end{cases} \tag{16a}$$

where $\dot{u}_i^S$ is the displacement rate of a point on the ECM located at $x_i - \Delta_i$. The second of the results in Eq. (16) formalizes the processes described in Appendix A. It follows that there is energy dissipation along the interface between the cell membrane and the ECM, resulting from the irreversible switching process (Appendix A). This is apparent in Fig. 7a where the hysteresis resulting from cyclic motion of the integrin is characterized by the dashed line in the force–displacement plot.

The irreversible integrin–ligand interaction mechanisms that occur for integrins on the ECM cannot occur for integrins outside the ECM periphery. Thus, as the integrin moves to the right away from the ECM,

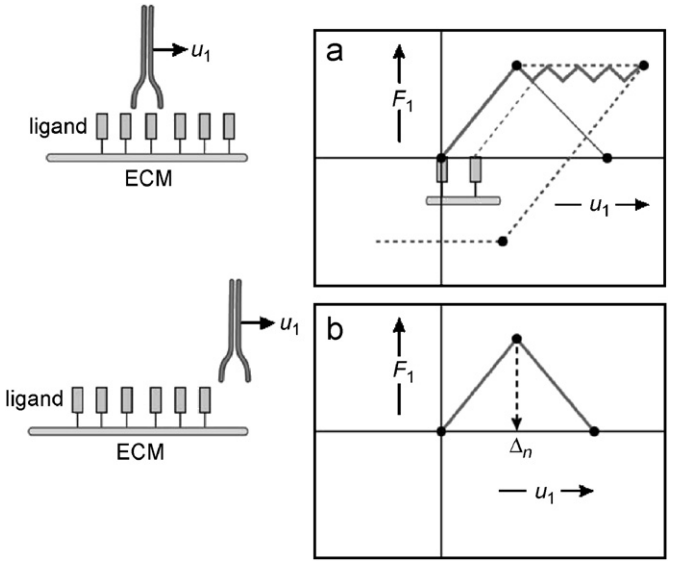

Fig. 7. Sketches of the force versus displacement relation for (a) a single integrin sliding over an ECM with a dense array of receptors and (b) integrin as it leaves the ECM periphery. For purposes of illustration we have taken $u_2 = 0$ and shown the force–displacement relationships assuming that $\Delta_1 = 0$ at $u_1 = 0$ in both (a) and (b).

eventually the integrin-ligand complex will rupture (Fig. 7b), and at this stage the surface energy will be created as the integrin moves further away from the rightmost ligand, and the force relaxes to zero. We assume that, for such integrins, the rate of change of the stretch is equal to the relative displacement rate between the integrin and the corresponding ligand on the ECM, i.e.

$$\dot{\Delta}_i = \dot{u}_i - \dot{u}_i^{\mathrm{S}}. \tag{16b}$$

This condition invokes the force–displacement relation depicted in Fig. 7b as the integrin moves beyond the edge of the ECM. Note that for a rigid ECM the substrate displacements are zero and thus $\dot{u}_i^{\mathrm{S}} = 0$.

4. Parameters for a one-dimensional model

We illustrate the features of the model by considering a one-dimensional cell, thickness $b = 1\,\mu\mathrm{m}$ (Fig. 8), on a rigid ECM. The active contractile response is modeled using the one-dimensional version of the cytoskeleton constitutive law proposed by Deshpande et al. (2007), summarized in Appendix B. The contractile properties of the cell are fixed at those employed in Deshpande et al. (2006, 2007): namely, the decay constant of the activation signal for the stress fiber formation is, $\theta = 720$ s, while the passive Young's modulus is $E = 0.08\,\mathrm{kPa}$. The non-dimensional reaction rate constants are $\bar{k}_{\mathrm{f}} = 10$ and $\bar{k}_{\mathrm{b}} = 1.0$ while the non-dimensional fiber rate-sensitivity is, $\bar{k}_{\mathrm{v}} = 10$. The maximum tension exerted by the stress fibers is, $\sigma_{\max} = 4.0\,\mathrm{kPa}$, and the reference strain rate in the cross-bridge dynamics law, $\dot{\varepsilon}_0 = 2.8 \times 10^{-4}\,\mathrm{s}^{-1}$. Thus, the non-dimensional cytoskeletal properties are: $\bar{E} \equiv E/\sigma_{\max} = 0.02$, $\bar{k}_{\mathrm{f}} = 10$, $\bar{k}_{\mathrm{b}} = 1$, $\bar{k}_{\mathrm{v}} = 10$, $\dot{\bar{\varepsilon}}_0 \equiv \dot{\varepsilon}_0$, $\theta = 0.2$.

All results are presented at a temperature $T = 310\,\mathrm{K}$. The reference adhesion properties are specified in a manner that assures their consistency with accepted ranges of binder parameter values. The uniform density of integrins (high and low affinity taken together) in an isolated cell is denoted by ξ_0 and taken to be $5000\,\mathrm{integrins}\,\mu\mathrm{m}^{-2}$ while the mobility of the low affinity binder is, $\mathrm{m} = 10\,\mu\mathrm{m}^2\mathrm{s}^{-1}$ (Lauffenburger and Linderman, 1996). The difference in the reference chemical potentials of the high and low affinity integrins is taken to be $\mu_{\mathrm{H}} - \mu_{\mathrm{L}} = 5\,\mathrm{kT}$ such that the ratio $\xi_{\mathrm{L}}/\xi_{\mathrm{H}} \approx 150$ for a cell with contractility curtailed ($F_i = \Phi = 0$); consistent with observations (McCleverty and Liddington, 2003). Experimental measurements suggest that the

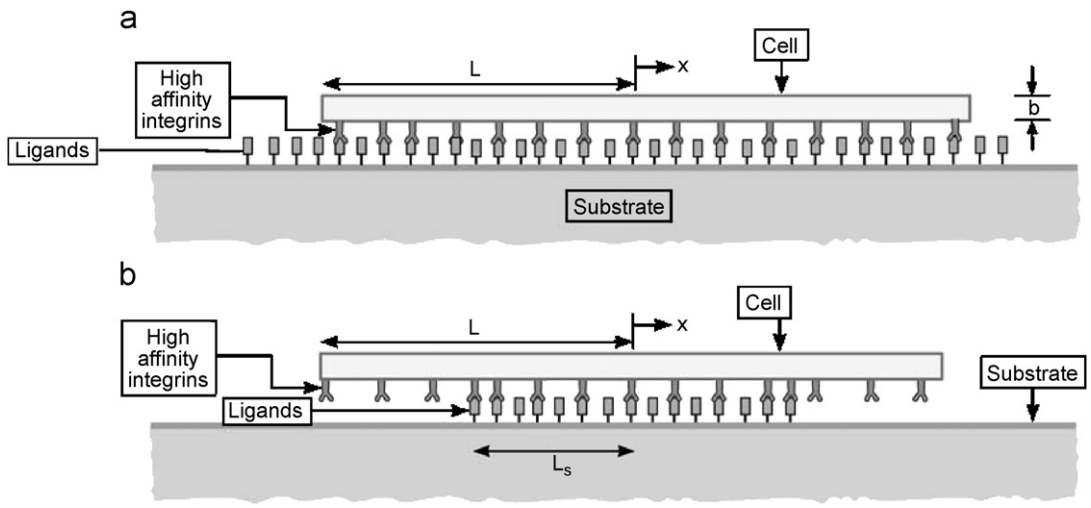

Fig. 8. The two one-dimensional cell adhesion problems analyzed. A cell of length $2L$ and thickness b on (a) an infinite ECM and (b) a patterned ECM with a ligand patch of length $2L_s$.

strength of the integrin-ligand complex varies in the range, $2 \rightarrow 10\,\mathrm{pN}$ (Rinko et al., 2004; Merkel et al., 1999), while the surface energy per integrin is in the range $5 \rightarrow 35\,\mathrm{kT}$ (Leckband and Israelachvili, 2001). We choose a reference stiffness, $\lambda_s = 0.15\,\mathrm{nN\,\mu m^{-1}}$, and stretch at the maximum force $\Delta_n = 13\,\mathrm{nm}$, such that the resultant maximum strength $\lambda_s\Delta_n$ and surface energy γ are consistent with the lower ends of the ranges quoted above. The reference adhesive properties in non-dimensional terms are then given as (i) surface energy $\bar{\gamma} \equiv \lambda_s\Delta_n^2/\mathrm{kT} = 6.2$, (ii) strength of integrin-ligand complex $\bar{\tau}_{\max} \equiv \lambda_s\Delta_n\xi_0\sqrt{\mathrm{mkT}\,\theta}/(\sigma_{\max}b) = 0.45$, and (iii) the difference in the reference potentials of the high and low affinity integrins, $\Delta\bar{\mu} = (\mu_H - \mu_L)/\mathrm{kT} = 5$.

In the following sections we consider two examples to illustrate some essential features that emerge upon coupling the new adhesion model with the existing cell contractility model (Deshpande et al., 2006, 2007).

5. A single cell on an "infinite" rigid substrate

5.1. Formulation

A one-dimensional cell, length $2L$ (along the x-direction), is bound to a long rigid ECM (Fig. 8a). With x the co-ordinate of a material point in the cell in the current configuration and X the corresponding co-ordinate in the undeformed configuration, the response of the cell is completely described by the following set of differential equations:

The one-dimensional mechanical equilibrium equation is

$$b\frac{\partial \Sigma}{\partial x} = \xi_H F, \tag{17a}$$

where F is the force exerted by the cell on the integrin–ligand complex, and Σ the stress in the cell, as specified by constitutive Eqs. (B.1)–(B.4) through the stress fiber concentration η.

The strain-rate $\dot{\varepsilon}$ in the cell is related to the displacement rates $\dot{u}$ of cell material points through the compatibility equation

$$\dot{\varepsilon} \equiv \frac{\partial \dot{u}}{\partial x} \tag{17b}$$

As the integrins are always in contact with the rigid ECM, the stretch rate is given by the one-dimensional version of Eq. (16):

$$\dot{\Delta} = \begin{cases} \dot{u}, & |\Delta| \leqslant \Delta_n \text{ or } \left[\dfrac{\partial \Phi}{\partial |\Delta|}\dot{\Delta} < 0\right], \\ 0, & \text{otherwise.} \end{cases} \tag{18a}$$

Since the effective stretch is $\Delta_e \equiv |\Delta|$, the integrin-ligand interaction force is given as

$$F = \begin{cases} \lambda_s \Delta, & |\Delta| \leqslant \Delta_n, \\ 2\lambda_s \Delta_n \text{sign}(\Delta) - \lambda_s \Delta & \Delta_n < |\Delta| \leqslant 2\Delta_n, \\ 0, & |\Delta| > 2\Delta_n. \end{cases} \tag{18b}$$

The potential Φ is obtained by replacing Δ_e with $|\Delta|$ in Eq. (15a).

The problem description is completed by specifying the one-dimensional trafficking equations for the concentration ξ_H of the high affinity integrins. From Eqs. (4), (7) and (12):

$$\frac{\partial \xi}{\partial t} = m \frac{\partial}{\partial x}\left(\xi_L \frac{\partial \chi_L}{\partial x}\right) - \xi \dot{\varepsilon}, \tag{19a}$$

where $\xi = \xi_L + \xi_H$, and

$$\chi_L = \mu_L + kT \ln \frac{\xi_L}{\xi_R} = \mu_H + \text{kT} \ln \frac{\xi_H}{\xi_R} + \Phi(\Delta) - F\Delta. \tag{19b}$$

For simplicity we assume that the cells are stress and stress fiber free at time $t = 0$: thus, $u = \eta = \varepsilon = \Sigma = 0$ with a single activation signal C imposed at $t = 0$. Moreover, since the cells are initially stress free, the high affinity integrin-ligand complexes are un-stretched such that $\Delta = 0$ everywhere on the cell surface. Then Eq. (19b) gives the uniform concentration of high and low affinity integrins over the cell surface at time $t = 0$ as

$$\xi_H = \frac{\xi_0}{1 + \xi_L/\xi_H}, \tag{20a}$$

and

$$\xi_L = \frac{\xi_0}{1 + \xi_H/\xi_L}, \tag{20b}$$

respectively, where

$$\frac{\xi_H}{\xi_L} = \exp\left[-\frac{\mu_H - \mu_L}{\text{kT}}\right]. \tag{21}$$

The stress and flux boundary conditions for Eqs. (17) and (19), respectively are

$$\Sigma = 0 \text{ and } j = -m\xi_L \frac{\partial \chi_L}{\partial x} = 0 \text{ at } X = \pm L. \tag{22}$$

Recall that the cell is symmetric about $X = 0$, so we only analyze the response over the domain $0 \leqslant X \leqslant L$ with symmetry boundary conditions ($u = 0$; $j = 0$) imposed at $X = 0$.

The finite element solution technique for these one-dimensional partial differential equations is detailed in Appendix C. All calculations use a mesh comprising 600 two-node elements with linear interpolation functions. The mesh is refined near the edge, $X = L$, in order to accurately capture large parameter gradients there.

5.2. The formation and growth of FAs

The resulting distributions of the high and low affinity integrins as a function of the normalized position $\bar{x} \equiv x/L$ are plotted in Figs. 9a and b, respectively, for a cell of length $L = 5\,\mu\text{m}$ (normalized length

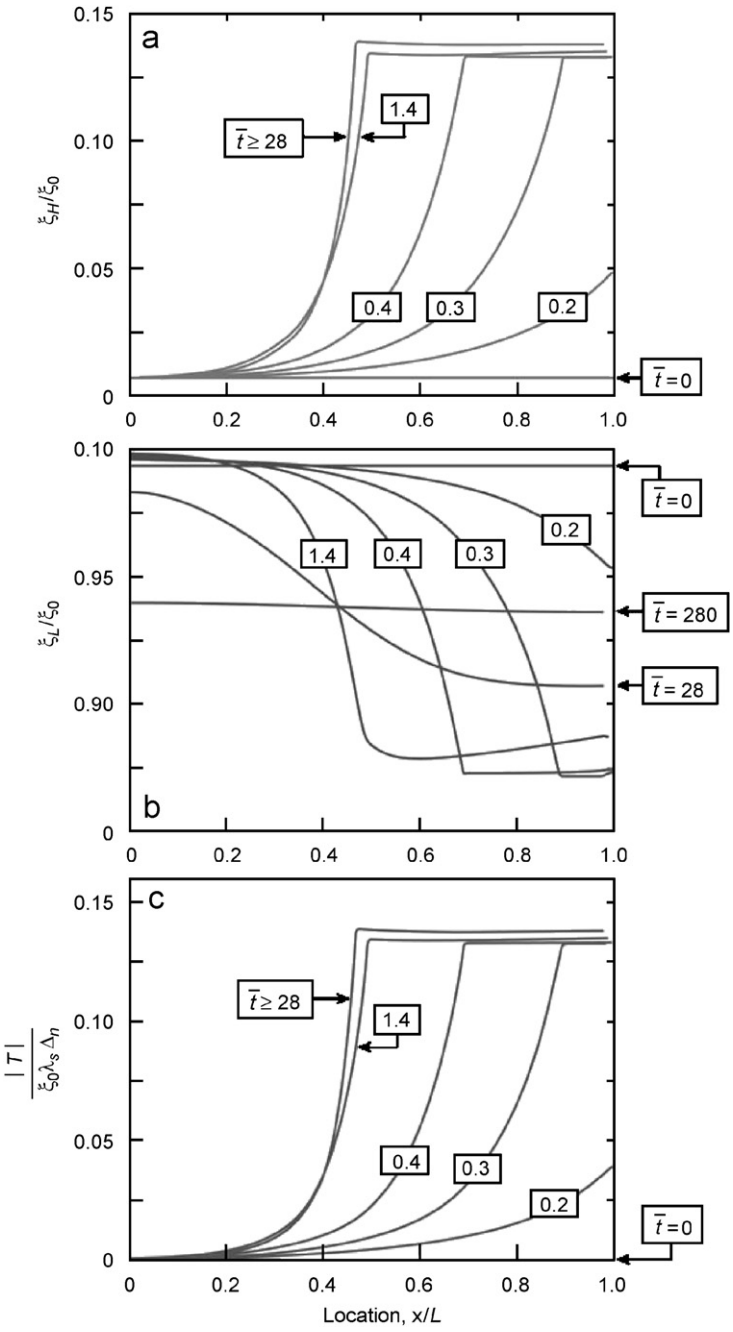

Fig. 9. Spatial distributions of the (a) high and (b) low affinity integrin concentrations and (c) normalized tractions exerted by the cell on the ECM at selected times after the application of the activation signal at $t = 0$ for the problem sketched in Fig. 8a. The cell length was taken as $L = 5\,\mu m$ ($\bar{L} = 28$) and reference properties were employed.

$\bar{L} \equiv L/\sqrt{mkT\theta} = 28$) at selected times, $\bar{t} \equiv t/\theta$. At time $\bar{t} = 0$, concentrations ξ_L/ξ_0 and ξ_H/ξ_0 are spatially uniform with $\xi_L/\xi_H \approx 150$, as specified by Eq. (21). The activation signal applied at $\bar{t} = 0$ initiates contractility in the cell resulting in the ensuing sequence of events.

Step I: Mechanical equilibrium dictates that high tractions $T = \xi_H F$ are developed near the cell edge, at $\bar{x} \approx 1$ (Fig. 9c shows the traction between the cell and the ECM as a function of position $\bar{x} \equiv x/L$ at various times $\bar{t} \equiv t/\theta$).

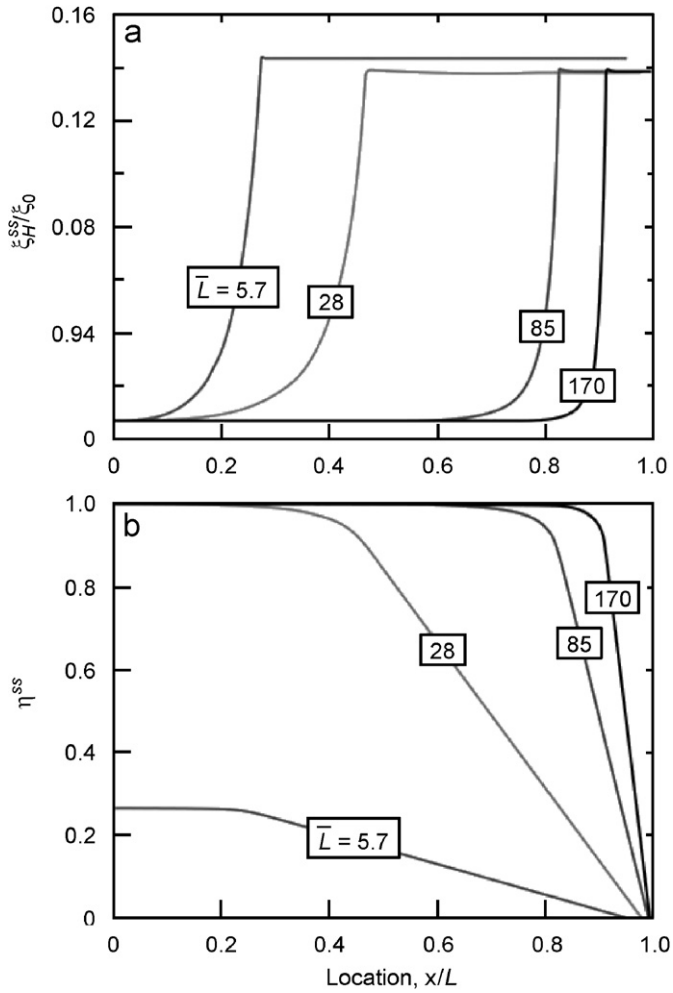

Fig. 10. The effect of cell size $\bar{L}$ on the steady-state (a) distributions ξ_H^{ss} of the high affinity integrins and (b) the distributions of the stress fiber concentrations η. The results are for the problem sketched in Fig. 8a with reference adhesion properties.

Step II. These high tractions reduce the chemical potentials of the high affinity integrins (Eq. (2)).

Step III. In order to maintain thermodynamic equilibrium, low affinity binders transform to their high affinity states at sites of high traction.

Step IV. This transformation reduces the concentration, ξ_L, of mobile, low affinity integrins, which initiates the diffusive flux of those binders toward the sites of high traction.

With increasing tractions, the concentrations of the high affinity binders increases and thus the stiffness per unit area, $\xi_H\lambda_s$, of the FAs increases. This increase further promotes the applied forces by inhibiting the dissociation of the stress fibers in the cytoskeletal contractility model (Deshpande et al., 2006), thereby further increasing the tractions applied by the cell on the ECM. *This co-operativity between contractility and FA formation is inherent in the model.*

FAs are identified by staining for proteins, such as vinculin. By equating ξ_H with the vinculin concentration, the model accurately predicts the experimental observation that the FAs concentrate around the cell periphery (Chen et al., 2003). Moreover, without contractility, the low focal adhesion concentrations predicted by the model (see time $\bar{t} = 0$ in Fig. 9a) are consistent with the observed reduction in vinculin concentration when contractility is curtailed by adding BDM into the culture (Chen et al., 2003) (see Fig. 1b).

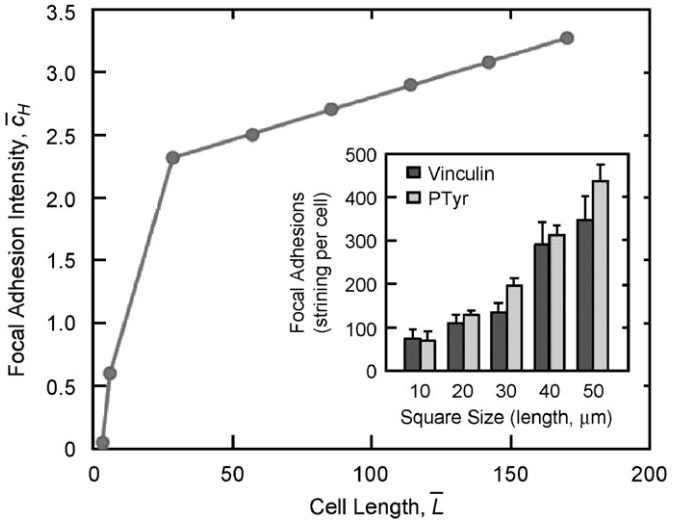

Fig. 11. The normalized total focal adhesion intensity $\bar{c}_{\mathrm{H}}$ at steady-state. The results are for the problem sketched in Fig. 8a with reference adhesion properties. Measurements of the total focal adhesion intensity from Chen et al. (2003) are included as an inset.

The predicted effect of cell size $\bar{L}$ on the distributions of the high affinity integrin concentrations $\xi_{\mathrm{H}}^{\mathrm{ss}}$ at steady-state (Fig. 10a) is broadly consistent with the experimental observations (see Fig. 1a). Namely, the fraction of the cell area covered by a high concentration of FAs increases with decreasing cell size. The simplistic rationalization is that mechanical equilibrium would require a high concentration of FAs in a region near the cell edge of length

$$\ell \approx \frac{\sigma_{\max} b}{\xi_0 \lambda_{\mathrm{s}} \Delta_n}. \tag{23}$$

This length is independent of the cell size L and *thus* ℓ/L *increases with decreasing* L. However, this rationale neglects the co-operativity between cell contractility and FA formation. These effects are highlighted in Fig. 10b where the steady-state spatial distributions of the stress fiber concentrations η^{ss} are plotted for the cases considered in Fig. 10a. The fraction of the cell covered by a high concentration of stress fibers increases with increasing L. Moreover, for the smallest cell ($\bar{L} = 5.7$) full polymerization ($\eta^{\mathrm{ss}} = 1$) of the stress fibers is not achieved even at the center of the cell, because the "effective" substrate stiffness felt at the cell center decreases with decreasing L.

The total normalized FA intensity at steady-state is defined as

$$\bar{c}_{\mathrm{H}} \equiv \frac{c_{\mathrm{H}}}{\xi_0 \sqrt{mkT\theta}}, \tag{24a}$$

where

$$c_{\mathrm{H}} = \int_0^L \xi_{\mathrm{H}}^{\mathrm{ss}} \, \mathrm{d}X. \tag{24b}$$

The variation of $\bar{c}_{\mathrm{H}}$ with normalized cell size $\bar{L}$ is included in Fig. 11. Evidently, the model predicts that the total FA intensity increases with increasing cell size. This prediction is consistent with observations (Chen et al., 2003) for Bovine capillary endothelial cells (inset in Fig. 11) that the total vinculin and phosphotyrosine quantities increase as the side length of a square cell on a patterned substrate increases.

The effect of bond strength $\bar{\tau}_{\max}$ on the steady-state distributions of $\xi_{\mathrm{H}}^{\mathrm{ss}}$ is illustrated in Fig. 12a for a cell of length $\bar{L} = 28$ and three selected values of $\bar{\tau}_{\max}$ (with other properties held fixed at their reference values). Note that changing $\bar{\tau}_{\max}$ while keeping $\bar{\gamma}$ fixed requires that the values of λ_{s} and Δ_n be changed simultaneously. The main effect of reducing $\bar{\tau}_{\max}$ is to increase the fraction of the cell covered by a high concentration of focal

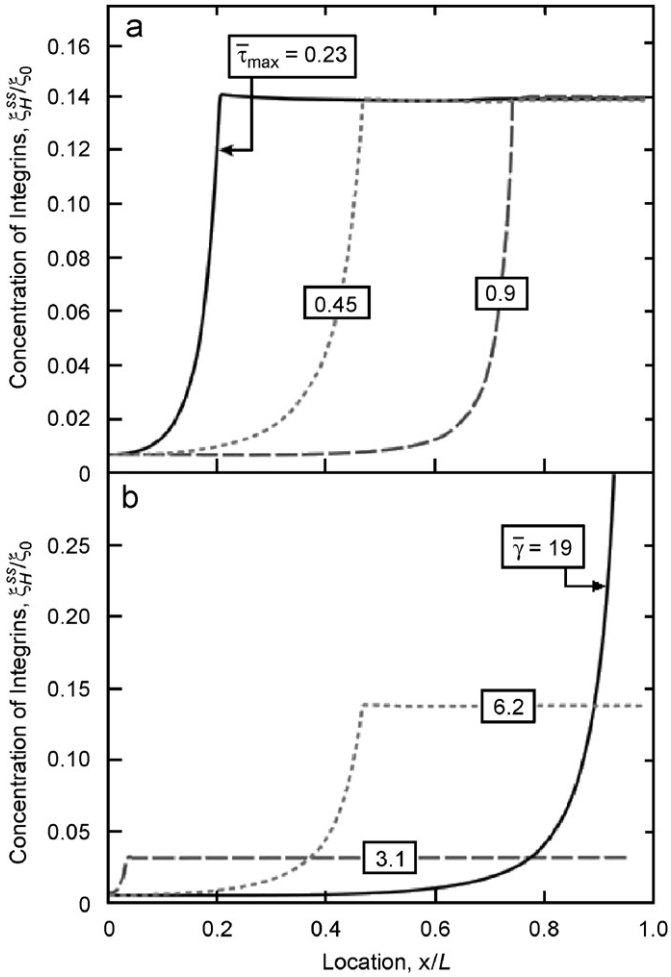

Fig. 12. The effect of (a) normalized bond strength $\bar{\tau}_{max}$ and (b) surface energy $\bar{\gamma}$ on the steady-state distributions of ξ_H^{ss} of the high affinity integrins for the problem sketched in Fig. 8a with $\bar{L} = 28$. Unless otherwise specified, the normalized properties are kept fixed at their reference values.

adhesions [as predicted by the scaling argument in Eq. (23)]. But $\bar{\tau}_{max}$ has negligible effect on the maximum value of ξ_H^{ss} because the thermodynamic equilibrium between the low and high affinity binders is primarily governed by the rupture energy γ of the integrin complex (kept constant in Fig. 12a). *The effect of surface energy* $\bar{\gamma}$ on the steady-state distributions of ξ_H^{ss} is shown in Fig. 12b for three selected values of $\bar{\gamma}$. Decreasing $\bar{\gamma}$ not only increases the fraction of the cell covered by a high concentration of focal adhesions, but also reduces the maximum values of ξ_H^{ss} for the reasons discussed above.

Cell adhesion is typically thought to be either governed by the diffusion of the integrins or by the receptor–ligand kinetics (Boulbitch et al., 2001). In order to illustrate the *effect of low affinity integrin mobility* we re-arrange the non-dimensional groups so that the binder mobility only appears in the non-dimensional cell length, $\bar{L} \equiv L/\sqrt{mkT\theta}$, and thus re-define the non-dimensional integrin-ligand complex strength as, $\xi_0\lambda_s\Delta_n L/(\sigma_{max}b)$. The steady-state distributions of ξ_H^{ss} are included in Fig. 13 for two values of $\bar{L}$ and two of $\xi_0\lambda_s\Delta_n L/(\sigma_{max}b)$ with all other non-dimensional groups held fixed at their reference values. Increasing the binder mobility by about a factor of 15 (by decreasing $\bar{L}$ from 28 to 2) only slightly increases the FA concentrations, as parameterized by ξ_H^{ss} for a fixed strength $\xi_0\lambda_s\Delta_n L/(\sigma_{max}b)$. This insensitivity arises because the kinetics of the stress fiber formation and dissociation are much faster than the diffusive processes. Namely,

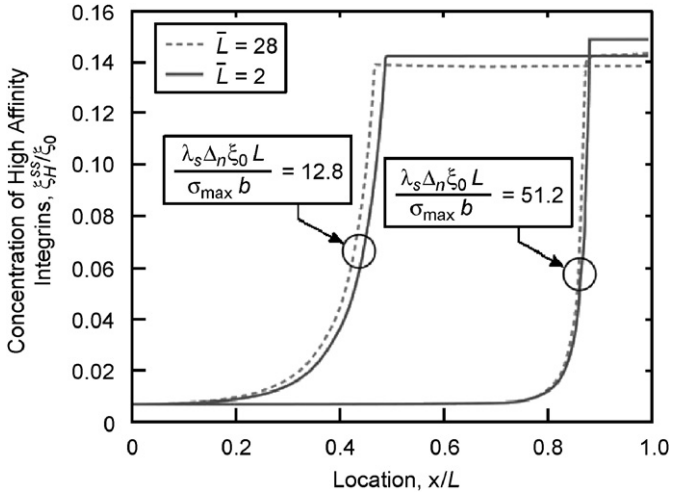

Fig. 13. The effect of low affinity integrin mobility on the steady-state distributions $\xi_{\mathrm{H}}^{\mathrm{ss}}$ of the high affinity integrins for the problem sketched in Fig. 8a. Results are shown for two choices of the normalized bond strengths $\xi_0\lambda_s\Delta_n L/(\sigma_{\max} b)$ with other normalized properties fixed at their reference values. The integrin mobility is parameterized using the normalized cell length such that a smaller $\bar{L}$ indicates a higher binder mobility.

the flux of the low affinity integrins is not fast enough to affect the stress fiber structure in the cell and adhesion is primarily governed by the cytoskeletal kinetics within the present framework.

6. A single cell on a patterned substrate

A cell on a patterned rigid substrate (Fig. 8b) mimics typical experimental situations wherein only a fraction of the cell is in contact with the ligand patch. The cell is symmetrically located such that the undeformed cell spans the domain $-L \leqslant X \leqslant L$, while the ligand patch is located over $-L_s \leqslant X \leqslant L_s$ where $L_s < L$. The governing equations require one addition. Now the integrins in the domain $|X| > L_s$ cannot continue to associate with the ligand molecules as they move further away from the ligand patch. For $|X| \leqslant L_s$, the evolution of the stretch Δ is given by Eq. (18a) and for $|X| > L_s$ by the one-dimensional version of Eq. (16b), $\dot{\Delta} = \dot{u}$. All results use the reference set of properties with $L_s = 5\,\mu\mathrm{m}$ and $L = 7\,\mu\mathrm{m}$. The boundary conditions employed are $\Sigma = 0$ and $j = 0$ at $X = L$ and symmetry boundary conditions ($j = u = 0$) at $X = 0$. The FE mesh comprised 800 and 320 two-noded elements over the domains $0 \leqslant X \leqslant L_s$ and $L_s < X \leqslant L$, respectively. The mesh was highly refined near the edges of the ligand patch. Unlike the situation in Fig. 8a, we cannot prescribe an initially stress-free configuration with a uniform distribution of integrins. Recall that binders located at $x \geqslant L_s + 2\Delta_n$ cannot be bound to receptors on the ECM and thus have energy $\Phi = \gamma$ and bond force $F = 0$. By contrast, binders located well within the ligand patch have un-stretched bonds with $\Delta = \Phi = F = 0$. Thus, the ratio of the concentrations of the high and low affinity integrins is higher over the region $0 \leqslant x \leqslant L_s$ than over $L_s < x \leqslant L$, with a transition zone developing around $x \approx L_s$. A procedure to set-up an initial equilibrium distribution of integrins in the passive cell (one that can sustain only elastic stresses and generate no stress fibers, $\eta = 0$, and hence no active stresses) is detailed in Appendix D.

An initial equilibrium distribution of the high affinity integrins is plotted in Fig. 14a. The transition zone occurs over a length approximately equal to Δ_n (Fig. 14b). The corresponding distributions of the bond lengths Δ of the high affinity integrins are plotted in Fig. 15a. Moving from the edge of the ligand patch towards the center of the cell, $|\Delta|$ decreases with $\Delta = 0$ for $x/L < 0.67$. By contrast, the bond length increases monotonically outside the ligand patch (over the region $L_s \leqslant x \leqslant L$): the sharp peak in concentration occurs at a bond stretch $|\Delta|\Delta_n$ when the term Φ–$F\Delta$ is at its minimum value ($-0.5\lambda_s\Delta_n^2$). As seen from Figs. 14 and 15a, this occurs at $x \approx L_s + \Delta_n$. The stretched integrin-ligand complexes exert tractions on the passive cell that are balanced by elastic straining: the spatial distributions of these strains are plotted in Fig. 15b. The cell is under

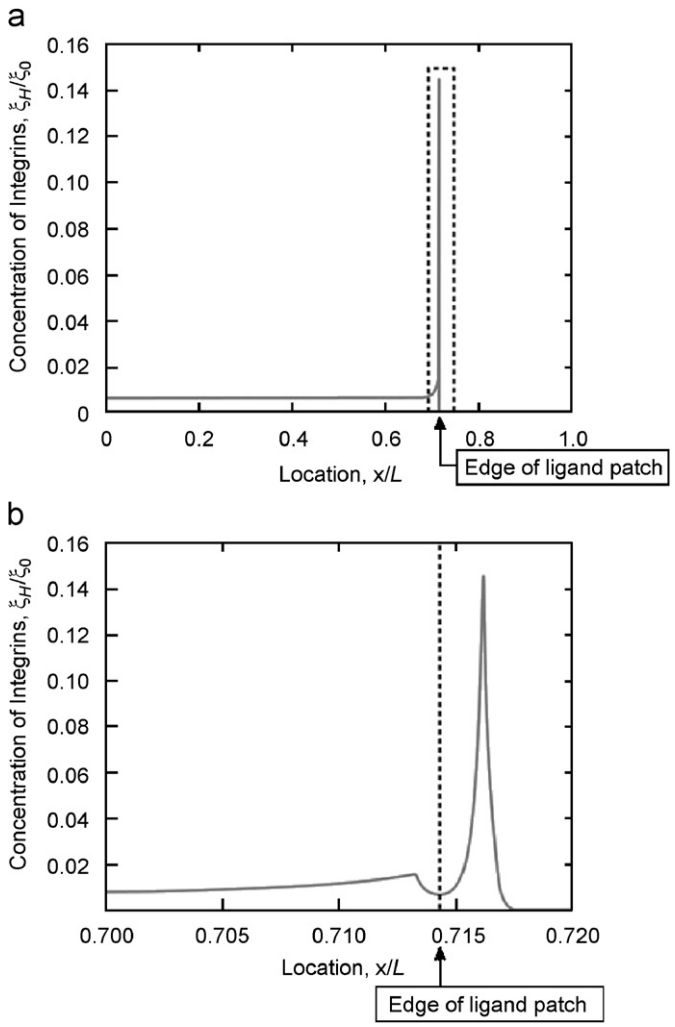

Fig. 14. (a) Initial ($\eta = 0$ and $\bar{t} = 0$) equilibrium distribution of the high affinity integrins ξ_H for a cell of length $L = 7\,\mu m$ on a ligand patch of length $L_s = 5\,\mu m$, and (b) magnified views of the distributions of ξ_H around the edge of the ligand patch. In (b) three additional initial distributions of ξ_H are used to illustrate the non-uniqueness of these initial distributions.

maximum compression near the edge of the ligand patch with the strains reducing to zero gradually for $x < L_s$. They are again zero for $x > L_s + 2\Delta_n$ when the tractions due to the integrin-ligand complex stretches are zero. As noted in Appendix D, this initial distribution of the integrins is not unique. Numerical investigations using the prescription in Appendix D have shown that differences, albeit rather small, in the distributions only occur in the transition zone around $x \approx L_s$. Subsequently, all results are shown for the initial integrin distribution plotted in Fig. 14a.

The resulting spatial distributions for the high affinity integrins at selected times after the application of the activation signal applied at time $t = 0$ is illustrated in Fig. 16a. Consistent with experimental observations (Fig. 1b) very low densities of FA are predicted at $t = 0$ when contractility due to stress fiber activation has not initiated. The initiation of contractility increases the FA density significantly with a steady-state established for $\bar{t} > 14$. The transition region near the edge of the ligand patch around $X = L_s$ (present in the initial distribution of the high affinity integrins Fig. 14a) persists even after the initiation of contractility: see the steady-state spatial distributions $\xi_H^{ss}(\bar{t} = 14)$ around the edge of the ligand patch included in Fig. 16b.

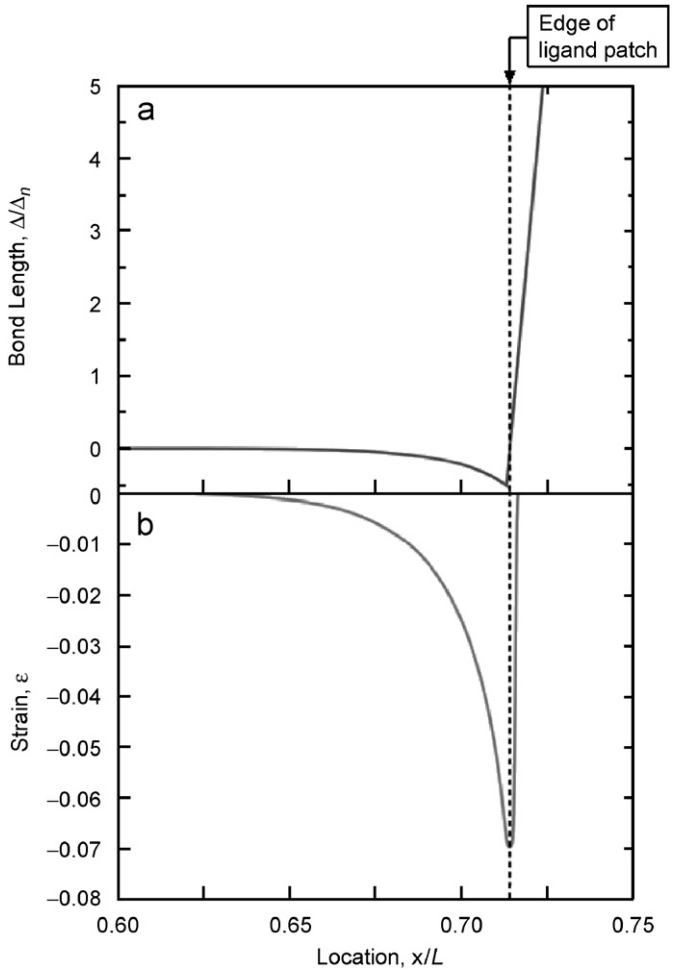

Fig. 15. The initial ($\eta = 0$ and $\bar{t} = 0$) spatial distributions of the (a) bond length and (b) strains for the integrin distributions of Fig. 14a.

7. Future perspectives

Early studies of cell adhesion on flat substrates described several distinct processes, including the initial clustering of integrins when they bind to ECM ligands, associated formation of FAs, and progressive maturation of these adhesion complexes as cells undergo active spreading and flattening. Because these processes proceed in parallel during initial attachment, it has been difficult to determine their interdependence. More recently, strategies have been devised that obviate these limitations. They include the patterning of ECM proteins on surfaces to control cell shape, while holding constant the ECM-coating density of ligands. They also implement a simultaneous biochemical strategy to control cell spreading independently of the total amount of ECM ligand in contact with the cell. For example, Parker et al. (2002) have shown that confining cells to square micro-patterns results in stress fibers and FA that concentrate at the cell corners. Additionally, Chen et al. (2003) have investigated scaling laws for the variations in the FA intensity with cell area for similar square cells. Such techniques have recently undergone significant refinements. In particular, Théry et al. (2006) have investigated the effect of cell shape on the distribution of actin and vinculin at fixed cell area, exemplified by Fig. 17, which visualizes the actin and vinculin distributions in a human retinal endothelial cell placed on a V-shaped fibronectin ligand pattern. Such studies indicate a complex interaction among cell shape, ligand patch geometry, and cytoskeletal response with strong stress fibers forming along the

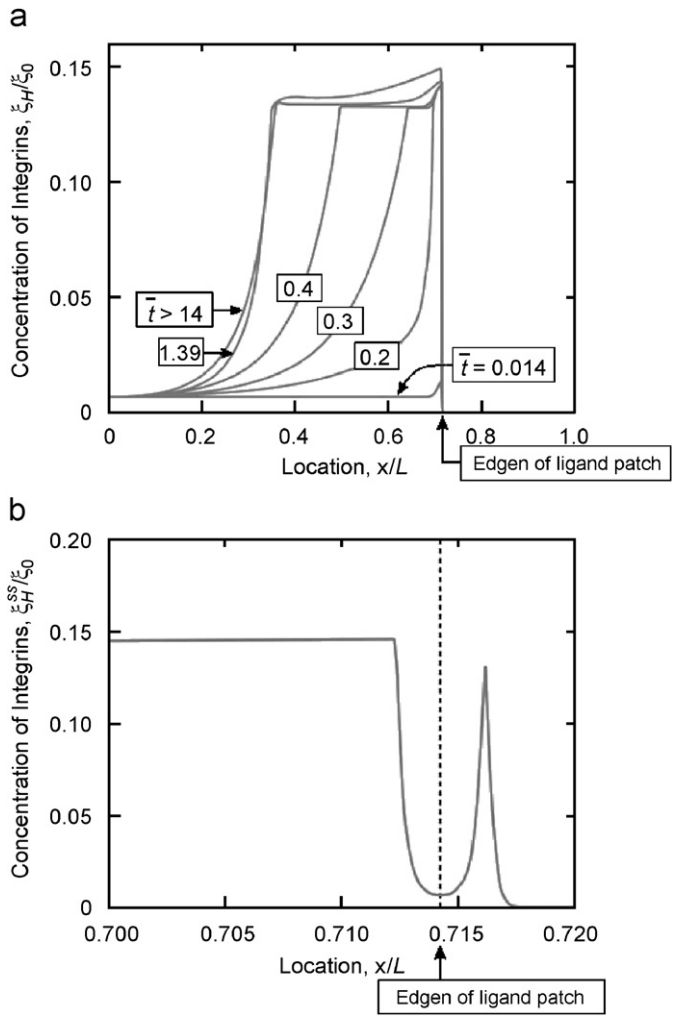

Fig. 16. (a) Spatial distributions of the high affinity integrins at selected times after the application of the activation signal at time $t = 0$. (b) Magnified view of the steady-state distributions ξ_H^{ss} around the edge of the ligand patch. Results are shown for the initial distribution ξ_H plotted in Fig. 14.

non-adhesive edges and high FA densities along the edges of the ligand patch. The coupled cytoskeletal contractility and FA model developed here is sufficiently general to enable us to make quantitative predictions of such experiments.

An initial two-dimensional prediction based on the current model from Pathak et al. (2007) is included in Fig. 17 which plots distributions of the high affinity integrin concentrations and distributions of the stress fiber density or equivalently actin density. Also included with the predicted stress fiber distributions are line segments showing the "effective" direction of the stress fiber. The predictions are remarkably consistent with observations: (i) since the cell exerts maximum tractions on the ECM near the edges of the ligand patch, high FA densities are predicted in this region and (ii) aligned stress fibers form along the non-adhesive edge; see Pathak et al. (2007) for details and interpretation of the analysis. Finally we note that the framework presented here is generic and can be extended to the full three-dimensional case by combining the present model with a three–dimensional traction–separation law for receptor-ligand binding as proposed recently by Liu et al. (2007).

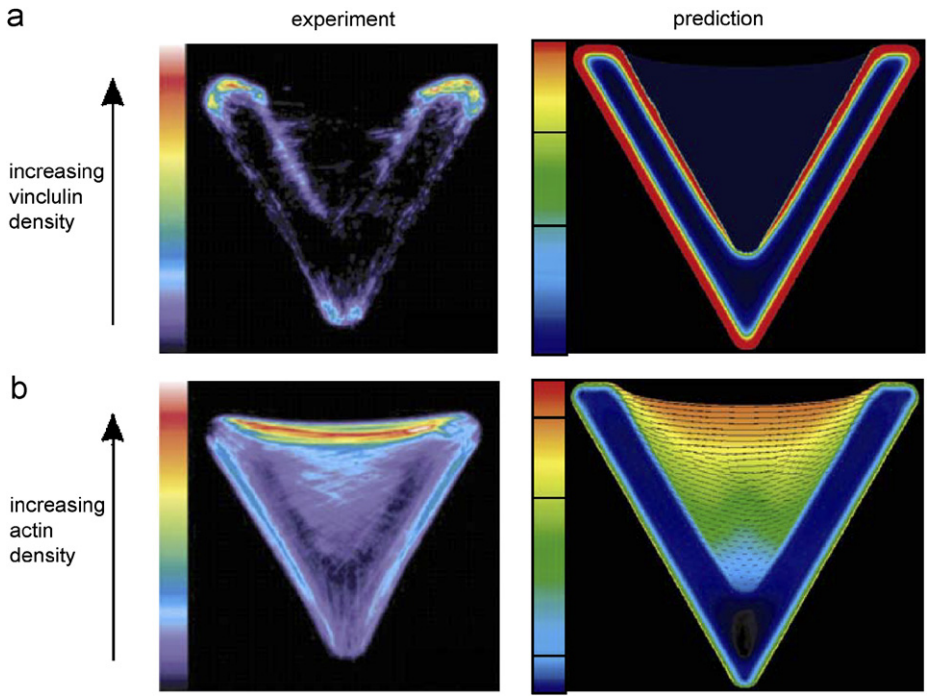

Fig. 17. Observations (averaged over 10 cells) and predictions of the (a) vinculin and (b) actin distributions in infinity telomerase-immortalised retinal pigment epithelial human cells placed on a V-shaped fibronectin pattern. The edge of the V is 46 μm. The observations are reproduced from Théry et al. (2006) while the predictions are from Pathak et al. (2007).

Acknowledgments

VSD acknowledges support from the Leverhulme Trust, UK. M.M., R.M.M. and A.G.E. thank the Army Research Office for their support through a Multidisciplinary University Research Initiative program on "Bio-Mechanical Interfaces for Cell-Based Microsystems", Prime Award No.: W911NF-04-1-071.

Appendix A. Sliding of integrins over an ECM with a high density of ligand molecules

Here we propose two mechanisms to rationalize the force displacement relation for integrins sliding over an ECM with a high density of ligand molecules.

Mechanism 1 (Fig. A1): Take as a starting point the configuration in which the high affinity integrins and the ligand molecules form complexes in an unstretched configuration (state a). Upon applying a force the cell membrane displaces to the right. The force reaches a peak as the high affinity integrin–ligand complexes become highly stretched (state b). Further stretching of the complexes would decrease the forces. The chemical potential χ_H is lowest when the force in the integrin–ligand complex attains its maximum (Fig. 3). It is now energetically favorable for the high and low affinity integrins to "switch". Compare states b and c where (at a fixed cell membrane displacement) the high affinity integrins dissociate from the ligand molecules and covert to the low affinity state, while simultaneously nearby low affinity integrin molecules convert to the high affinity state and form complexes with the ligand molecules. Further displacement of the cell membrane results in the forces rising again (state d) and the process repeats. Thus, sliding of the cell membrane with respect to the substrate occurs at almost constant force.

Mechanism 2 (Fig. A2): All known shear processes in solids involve geometric imperfections. They are incapable of proceeding by rigid body displacement across the shear plane because the energy penalty is excessive. The imperfection enables the net shear to be attained by sequential, localized displacements that

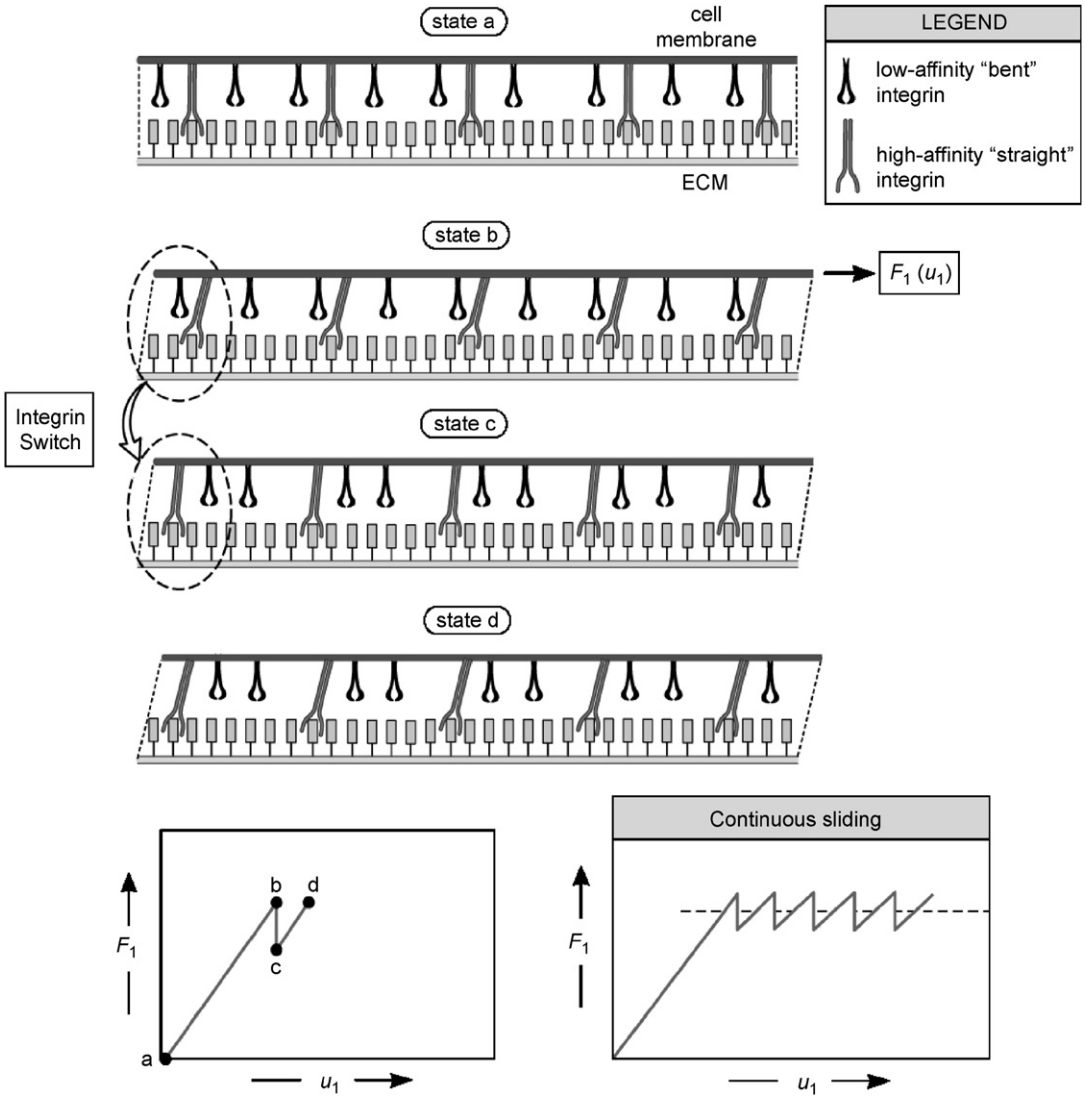

Fig. A1. Mechanism 1 for the sliding of integrins along an ECM with a high density of ligand molecules: switching between high and low affinity integrins.

translate along the plane. The most comprehensively characterized is the dislocation in crystalline solids (Hirth and Lothe, 1968). The analog for high affinity integrins (attached to the cell) shearing over the receptors on the ECM is depicted in Fig. A2. In this depiction one integrin is in an unattached location (the dislocation), while all others are attached. Initially, the dislocation is at the right end of the ensemble. Upon application of a force F, the dislocation moves from right to left. Once it has exited the ensemble at the left the cell has translated over the ECM by one unit. In order to accommodate the displacements around the dislocation, the cell must stretch locally, as indicated by the thinning of the membrane in Fig. A2. This local stretch zone translates with the dislocation. Since most of the integrins are bound to receptors, throughout, the cell sustains an average force with small oscillations during each unit translation of the dislocation. While the sketch on Fig. A2 illustrates the motion of a single geometric imperfection, we note that the mechanics and physics of dislocations in crystals provide a basis for understanding how dislocations form, multiply and allow repetitive shear straining.

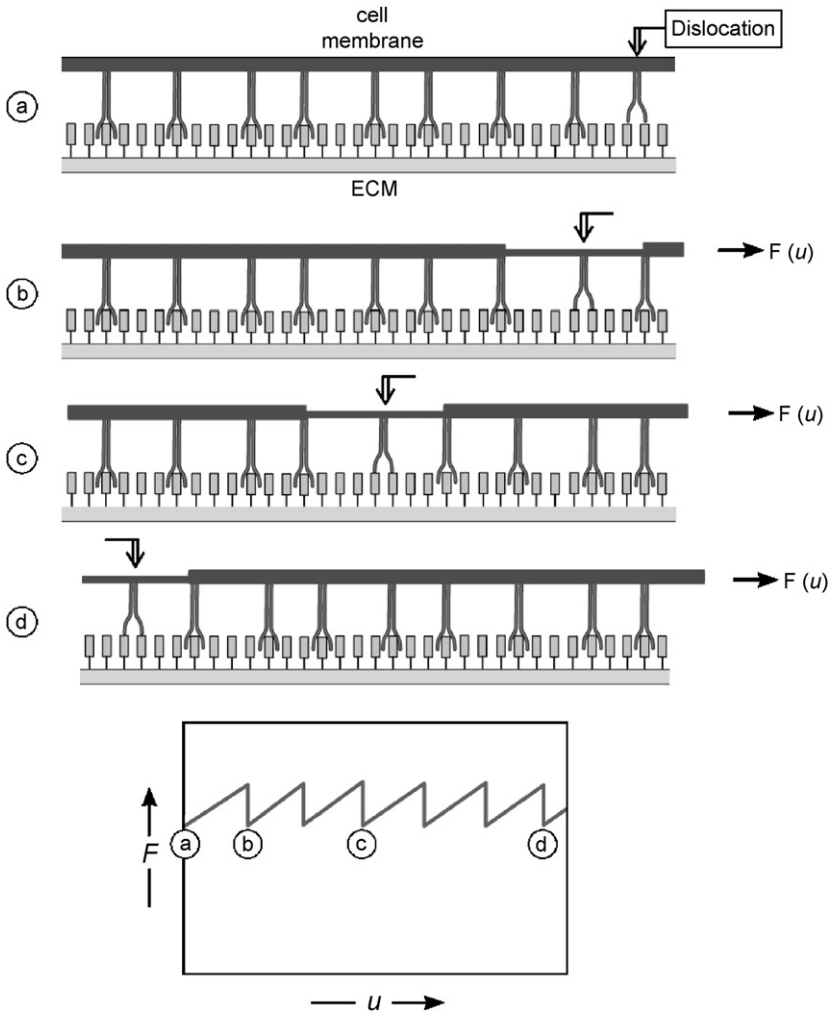

Fig. A2. Mechanism 2 for the sliding of integrins along an ECM with a high density of ligand molecules: the dislocation type mechanism.

Appendix B. The one-dimensional cytoskeletal model

A bio-chemo-mechanical model has been devised that captures the formation and dissociation of stress fibers, as well as the associated generation of tension and contractility (Deshpande et al., 2006, 2007). The stress fiber formation is initiated by a nervous impulse or a biochemical or mechanical perturbation that triggers a signaling cascade within the cell. We model this signal as an instantaneous spike of unit magnitude followed by an exponentially decaying pulse giving C (which may be thought of as the concentration of Ca^{2+}) as

$$C = \exp(-t_i/\theta), \tag{B.1}$$

where θ is the decay constant and t_i is the time after the onset of the most recent activation signal. The formation of stress fibers is parameterized by an activation level, designated η ($0 \leqslant \eta \leqslant 1$), defined as the ratio of the concentration of the polymerized actin and phosphorylated myosin within a stress fiber bundle to the maximum concentrations permitted by the biochemistry. The evolution of the stress fibers is characterized by a first-order kinetic equation:

$$\dot{\eta} = [1-\eta]\frac{C\bar{k}_{\mathrm{f}}}{\theta} - \left(1 - \frac{\sigma}{\sigma_0}\right)\eta\frac{\bar{k}_{\mathrm{b}}}{\theta}, \tag{B.2}$$

where the overdot denotes time-differentiation. In this formula, σ is the tension in the stress fiber bundle , while $\sigma_0 \equiv \eta\sigma_{\max}$ is the corresponding isometric stress at activation level η, with $\sigma_{\max}$ being the tensile stress at full activation ($\eta = 1$). The dimensionless constants $\bar{k}_f$ and $\bar{k}_b$ govern the rates of stress fiber formation and dissociation, respectively. In turn, the stress σ is related to the fiber contraction/extension strain rate $\dot{\varepsilon}$ by the cross-bridge cycling between the actin and myosin filaments. The simplified (but adequate) version of the Hill-like (Hill, 1938) equation employed to model these dynamics is specified as

$$\frac{\sigma}{\sigma_0} = \begin{cases} 0, & \dfrac{\dot{\varepsilon}}{\dot{\varepsilon}_0} < -\dfrac{\eta}{\bar{k}_v}, \\ 1 + \dfrac{\bar{k}_v}{\eta}\left(\dfrac{\dot{\varepsilon}}{\dot{\varepsilon}_0}\right), & -\dfrac{\eta}{\bar{k}_v} \leqslant \dfrac{\dot{\varepsilon}}{\dot{\varepsilon}_0} \leqslant 0, \\ 1, & \dfrac{\dot{\varepsilon}}{\dot{\varepsilon}_0} > 0, \end{cases} \tag{B.3}$$

where the rate sensitivity coefficient, $\bar{k}_v$, is the fractional reduction in fiber stress upon increasing the shortening rate by $\dot{\varepsilon}_0$.

The constitutive description for the cell is completed by including contributions from passive elasticity, attributed to intermediate filaments of the cytoskeleton attached to the nuclear and plasma membranes. These act in parallel with the active elements, whereupon additive decomposition gives the total stress:

$$\Sigma = \sigma + E\varepsilon, \tag{B.4}$$

where (for a linear passive response) E is Young's modulus and $\varepsilon \equiv \int_0^t \dot{\varepsilon}\,\mathrm{d}t$. In Section 5, we use only this one-dimensional version of the constitutive model that has been generalized to two and three dimensions by Deshpande et al. (2007).

Appendix C. Details of the finite element implementation

The numerical solution of the one-dimensional adhesion problem requires the coupled solution of the mechanical equilibrium Eq. (17) and the diffusion Eq. (19). We solve the weak forms of the partial differential Eqs. (17) and (19) using a finite element method in an updated-Lagrangian setting and couple them using a staggered approach as described below.

With boundary conditions $u = 0$ and $\Sigma = 0$ at $x = 0$ and $x = L_t$, respectively, the weak form of Eq. (17) at time t is given as

$$b\int_0^{L_t} \Sigma \frac{\partial \delta u}{\partial x}\,\mathrm{d}x = -\int_0^{L_t} \xi_H F \delta u\,\mathrm{d}x, \tag{C.1}$$

where L_t is the half-length of the cell at time t and δu are arbitrary variations of the displacements u. Similarly, using the boundary conditions $-m\partial\xi_L/\partial x = 0$ at $x = 0$ and $x = L_t$ (i.e. zero flux boundary conditions), the weak form of the diffusion Eq. (19) is written as

$$\int_0^{L_t} (1+\alpha)\frac{\partial \xi_L}{\partial t}\delta\xi_L\,\mathrm{d}x = -mkT\int_0^{L_t} \frac{\partial \xi_L}{\partial x}\frac{\partial \delta\xi_L}{\partial x}\,\mathrm{d}x - \int_0^{L_t} (1+\alpha)\xi_L\dot{\varepsilon}\delta\xi_L\,\mathrm{d}x - \int_0^{L_t} \dot{\alpha}\xi_L\delta\xi_L\,\mathrm{d}x, \tag{C.2}$$

where $\delta\xi_L$ are arbitrary variations of the concentrations of the low affinity integrins and

$$\alpha \equiv \exp\left(\frac{\mu_L - \mu_H - \Phi + F\Delta}{kT}\right). \tag{C.3}$$

We solve Eqs. (C.1) and (C.2) using a finite element method comprising 2-node elements with linear interpolation functions. Time integration of Eqs. (C.1) and (C.2) is performed using a fixed time step Δt as follows:

(i) Over the time step Δt, the concentrations ξ_H are assumed to remain fixed and the stresses, displacements and stretches Δ at time $t + \Delta t$ obtained by solving Eq. (C.1) using a Newton–Raphson scheme. Here, the

constitutive equations for Σ (as specified in Appendix B) are integrated from t to $t+\Delta t$ using a adaptive time-stepping 5th order Runge–Kutta scheme[3] with an integration tolerance of $\varepsilon_k = 0.001$.

(ii) The concentrations ξ_H and ξ_L are then updated over the time interval Δt by integrating the spatially discretized version of Eq. (C.2) with an adaptive 5th order Runge–Kutta scheme again with $\varepsilon_k = 0.001$. In performing this integration we assume that the strain rate $\dot{\varepsilon}$ remains constant over the time interval Δt, while the stretch Δ varies linearly from its value at t to $t+\Delta t$.

A displacement based convergence criterion given by

$$|c_{max}| \leqslant \varepsilon_r |\Delta u_{max}|, \tag{C.4}$$

was adopted for the Newton–Raphson scheme in the solution of Eq. (C.1). Here c_{max} is the largest change in the displacement degree of freedom of any node in the current Newton iteration and Δu_{max} is the maximum incremental change in the displacement degree of freedom of any node over the current time increment. The tolerance ε_r was set to 0.005 in all calculations.

Note that here we have used a staggered solution approach, where the concentrations ξ_H are assumed to remain fixed while integrating Eq. (C.1) over a time interval Δt. Numerical experimentation revealed that such an approach suffices for the parameter range used in this study with time steps $\Delta t < 5.0$ s. Recall that the time-scales associated with the diffusion process are much larger than those associated with the stress fiber kinetics for the parameters employed here and thus, such a decoupling of the mechanical equilibrium equation from the diffusion equation gives sufficiently accurate results. In all calculations presented here we employ a time step $\Delta t < 1.0$ s.

Appendix D. Specification of initial conditions for a cell on a patterned substrate

The integrins distributed over the cell membrane interact with the ECM and their initial distribution depends on the mechanical and chemical loading history that the cell has been subjected to. Here we do not consider the details of this history but instead, given a set of cell properties, choose a set of initial conditions that satisfy the following basic criteria:

(i) the low and high affinity integrins are in thermodynamic equilibrium $\chi_L - \chi_H = 0$ at every point on the cell membrane,
(ii) the low affinity integrins are in thermodynamic equilibrium spatially, i.e. the flux $j = 0$ at all points on the cell surface, and
(iii) the cell is in mechanical equilibrium.

In addition, we require that there are no spatial discontinuities in the concentration of the high affinity integrins (or equivalently in the stretches Δ) and thus specify that the gradients $\partial\xi_H/\partial x$ (and $\partial\Delta/\partial x$) are well defined over the cell surface. This constraint is rationalized by noting that an "ordered" (or equivalently low entropy) distribution corresponding to step changes in ξ_H or Δ is unlikely to result from an arbitrary mechanical and chemical loading of the cell for time $t<0$ as the system is expected to maximize its entropy. Note that these constraints do not specify a unique initial state, given a cell and substrate geometry and material properties. Rather the mechanical and chemical loading history will determine the precise initial conditions.

The initial conditions used in the results in Section 4.2 and plotted in Fig. 14 were obtained using the following relaxation scheme. The cell is modeled as an elastic solid and the stretches specified as

$$\Delta = \begin{cases} 0, & \text{if } |X| \leqslant (1-\varsigma)L_s \\ X - \text{sign}(X)(1-\varsigma)L_s & \text{otherwise,} \end{cases} \tag{D.1}$$

where the non-dimensional parameter ς varies between $0 \leqslant \varsigma \leqslant \Delta_n/L_s$. The corresponding densities of the high and low affinity integrins are then given in Eqs. (20a) and (20b), respectively. Thermodynamic

[3]Numerical Recipes in FORTRAN 77, The Art of Scientific Computing, 1993, Cambridge University Press.

equilibrium between the high and low affinity integrins requires that $\xi_H/\xi_L = \alpha$, as specified by Eq. (C.3). A configuration in mechanical equilibrium (boundary conditions $u = 0$ at $X = 0$ and $\Sigma = 0$ at $X = L$) is then obtained by solving Eq. (C.1) without permitting the diffusive flux of the low affinity integrins. Thus, Eq. (C.1) reduces to

$$b\int_0^{L_t}\sum\frac{\partial\delta u}{\partial x}\,\mathrm{d}x = -\int_0^{L_t}\frac{\xi_0}{1+\alpha}F\delta u\,\mathrm{d}x, \tag{D.2}$$

with α given in Eq. (C.3) and for the elastic cell $\Sigma = E\varepsilon$. The outcome is a system in mechanical equilibrium but with a spatially non-uniform distribution of low affinity integrins. This system is allowed to relax by solving the coupled mechanical equilibrium and diffusion equations as detailed in Appendix C, but with the cell modeled as a linear elastic solid. The final initial conditions to the simulations of Section 5.2 are obtained when a spatially uniform distribution of low affinity integrins emerges. The initial distribution of the high affinity binders plotted in Fig. 14 is obtained using $\varsigma = \Delta_n/L_s$.

References

Balaban, N.Q., Schwarz, U.S., Riveline, D., Goichberg, P., Tzur, G., Sabanay, I., Mahalu, D., Safran, S., Bershadskay, A., Addadi, L., Geiger, B., 2001. Force and focal adhesion assembly: a close relationship studied using elastic micropatterned substrates. Nat. Cell Biol. 3, 466–472.

Bell, G.I., 1978. Models for the specific adhesions of cells to cells. Science 200, 618–627.

Bell, G.I., Dembo, M., Bongrand, P., 1984. Cell adhesion. Biophys. J. 45, 1051–1064.

Bershadsky, A.D., Balaban, N.Q., Geiger, B., 2003. Adhesion dependent cell mechanosensitivity. Annu. Rev. Cell Dev. Biol 19, 677–695.

Boulbitch, A., Guttenberg, Z., Sackmann, E., 2001. Kinetics of membrane adhesion mediated by ligand-receptor interaction studied with a biomimetic system. Biophys. J 81, 2743–2751.

Brock, A., Chang, E., Ho, C.-C., Leduc, P., Jiang, X., Whitesides, G.M., Ingber, D.E., 2003. Geometric determinants of directional cell motility revealed using microcontact printing. Langmuir 19, 1611–1617.

Burridge, K., Chrzanowska-Wodnicka, M., 1996. Focal adhesions, contractility and signaling. Annu. Rev. Cell Dev. Biol. 12, 463–469.

Carman, C.V., Springer, T.A., 2003. Integrin avidity regulation: are changes in affinity and conformation underemphasized? Curr. Opinion Cell Biol. 15, 547–556.

Chen, C.S., Alonso, J.L., Ostuni, E., Whitesides, G.M., Ingber, D.E., 2003. Cell shape provides global control of focal adhesion assembly. Biochem. Biophys. Res. Commun. 307, 355–361.

Cluzel, C., Saltel, F., Lussi, J., Paulhe, F., Imhof, B.A., Wehrle-Haller, B., 2005. The mechanisms and dynamics of $\alpha v\beta 3$ integrin clustering in living cells. J. Cell Biol. 171, 383–392.

Dembo, M., Torney, D.C., Saxman, K., Hammer, D., 1988. The reaction-limited kinetics of membrane-to-surface adhesion and detachment. Proc. R. Soc., B 234, 55–83.

Deshpande, V.S., McMeeking, R.M., Evans, A.G., 2006. A bio-chemo-mechanical model for cell contractility. Proc. Nat. Acad. Sci. USA 103, 14015–14020.

Deshpande, V.S., McMeeking, R.M., Evans, A.G., 2007. A model for the contractility of the cytoskeleton including the effects of stress fiber formation and dissociation. Proc. R. Soc., London, A 463, 787–815.

Evans, E.A., 1985. Detailed mechanics of membrane-membrane adhesion and separation. I. Continuum of molecular cross-bridges. Biophys. J. 48, 175–183.

Freund, L.B., Lin, Y., 2004. The role of binder mobility in spontaneous adhesive contact and implications for cell adhesion. J. Mech. Phys. Solids 52, 2455–2472.

Gaskell, D.R., 1973. Introduction to Metallurgical Thermodynamics. McGraw-Hill.

Hill, A.V., 1938. The heat of shortening and the dynamic constants of muscle. Proc. R. Soc., London. B 126, 136–195.

Hirth, J.P., Lothe, J., 1968. Theory of Dislocations. McGraw-Hill, New York.

Hotchin, N.A., Hall, A., 1995. The assembly of integrin adhesion complexes requires both extracellular matrix and intracellular Rho/Rac GTPases. J. Cell Biol. 131, 1857–1865.

Hynes, R.O., 1992. Integrins: versatility, modulation and signalling in cell adhesion. Cell 69, 11–25.

Irvine, D.J., Hue, K.-A., Mayes, A.M., Griffith, L.G., 2002. Simulations of cell-surface integrin binding to nanoscale clustered adhesion ligands. Biophys. J. 82, 120–132.

Lauffenburger, D.A., Linderman, J., 1996. Receptors. Models for Binding, Trafficking, and Signaling. Oxford University Press, UK.

Leckband, D., Israelachvili, J., 2001. Intermolecular forces in biology. Q. Rev. Biophys. 34, 105–267.

Lennard-Jones, J.E., 1931. Cohesion. Proc. Phys. Soc. 43, 461–482.

Liu, P., Zhang, Y.W., Cheng, Q.H., Lu, C., 2007. Simulations of the spreading of a vesicle on a substrate surface mediated by receptor–ligand binding. J. Mech. Phys. Solids. 55, 1166–1181.

Lodish, H., Berk, A., Matsudaira, P., Kaiser, C.A., Krieger, M., Scott, M.P., Zipursky, S.L., Darnell, J., 2004. Molecular Cell Biology. W.H. Freeman & Co., USA.

Malvern, L.E., 1969. Introduction to the mechanics of a continuum medium. Prentice-Hall, Englewood Cliffs, NJ, USA.
McCleverty, C.J., Liddington, R.C., 2003. Engineered allosteric mutants of the integrin αMβ2 I domain: structural and functional studies. Biochem. J. 372, 121–127.
Merkel, R., Nassoy, P., Leung, A., Ritchie, K., Evans, E., 1999. Energy landscapes of receptor–ligand bonds explored with dynamic force spectroscopy. Nature 397, 50–53.
Mullins, W.W., 1957. Theory of thermal grooving. J. Appl. Phy. 28, 333–339.
Nicolas, A., Safran, S.A., 2006. Limitation of cell adhesion by the elasticity of the extracellular matrix. Biophys. J. 91, 61–73.
Nicolas, A., Geiger, B., Safran, S.A., 2004. Cell mechanosensitivity controls the anisotropy of focal adhesions. Proc. Nat. Acad. Sci. USA 101, 12520–12525.
Novak, I.L., Slepchenko, B.M., Mogilner, A., Loew, L.M., 2004. Cooperativity between cell contractility and adhesion. Phys. Rev. Lett. 93, 268109-1–268109-4.
Parker, K.K., Brock, A.L., Brangwynne, C., Mannix, R.J., Wang, N., Ostuni, E., Geisse, N.A., Adams, J.C., Whitesides, G.M., Ingber, D.E., 2002. Directional control of lamellipodia extension by constraining cell shape and orienting cell tractional forces. FASEB J 16, 1195–1204.
Pathak, A., Deshpande, V.S., McMeeking, R.M., Evans, A.G., 2007. Analysis of stress fiber and focal adhesion distributions of cells on micro-patterned substrates. J. R. Soc Interface, to appear.
Petroll, W.M., Ma, L., Jester, J.V., 2003. Direct correlation of collagen matrix deformation with focal adhesion dynamics in living corneal fibroblasts. J. Cell Sci. 116, 1481–1491.
Rinko, L.J., Lawrence, M.B., Guilford, W.H., 2004. The molecular mechanics of P- and L-selectin lectin domains binding to PSGL-1. Biophy. J. 86, 544–554.
Shemesh, T., Geiger, B., Bershadsky, A.D., Kozlov, M.M., 2005. Focal adhesions as mechanosensors: a physical mechanism. Proc. Nat. Acad. Sci. USA 102, 12383–12388.
Tan, J.L., Tien, J., Pirone, D.M., Gray, D.S., Bhadriraju, K., Chen, C.S., 2003. Cells lying on a bed of microneedles: an approach to isolate mechanical force. Proc. Nat. Acad. Sci. USA 100, 1484–1489.
Théry, M., Pépin, A., Dressaire, E., Chen, Y., Bornens, M., 2006. Cell distribution of stress fibres in response to the geometry of the adhesive environment. Cell Motil. Cytoskeleton 63, 341–355.
Wei, Z., Deshpande, V.S., McMeeking, R.M., Evans, A.G., 2007. Analysis and interpretation of stress fiber organization in cells subject to cyclic stretch. J. Biomech. Eng. ASME, to appear.
Xiao, T.J., Takagi, B.S., Coller, J.-H., Wang, Springer, T.A., 2004. Structural basis for allostery in integrins and binding to fibrinogen-mimetic therapeutics. Nature 432, 59–67.
Zhu, C., Bao, G., Wang, N., 2000. Cell mechanics: mechanical response, cell adhesion, and molecular deformation. Ann. Rev. Cell and Dev. Biol. 02, 189–226.